https://doi.org/10.5194/essd-2026-672
Preprint. Discussion started: 4 November 2026
© Author(s) 2026. CC BY 4.0 License.



Open Access Earth System Science Data Discussions

Simulation database for impact studies of the NGGM and MAGIC gravity missions

Marius Schlaak[1,2], Julia Pfeffer[3], Roland Pail[1], Marie Bouih[3], Alejandro Blazquez[2], Benoit Meyssignac[2], and Ilias Daras[4]

[1]Institute for Astronomical and Physical Geodesy, Technical University of Munich, Munich, Germany
[2]Université de Toulouse, LEGOS (CNES, CNRS, IRD, UT), 31400 Toulouse, France
[3]Magellium, 31520, Ramonville Saint-Agne, France
[4]ESA/ESTEC, Noordwijk, Netherlands

Correspondence: Marius Schlaak (marius.schlaak@tum.de)

Abstract. The ESA-SING dataset provides simulated satellite gravity products for three future gravimetry mission constellations: GRACE-C-like, NGGM, and MAGIC. The dataset is developed in the frame of the ESA SING project (www.esa-sing.org) and is based on the ESA Earth System Model 2.0. For the first time, the ESA SING dataset delivers simulated gravity products (L2 & L3) consistently generated over a 12-year period, including a wide range of mass redistribution processes as well as mission-specific errors, arising from instrumental noise and background model errors. In addition to the simulated gravity fields and their residual errors, static empirical variance-covariance matrices for 5-day and 30-day solutions, derived from Monte Carlo simulations, enable the assessment of the expected mission uncertainties. The dataset enables users to assess the impact of future satellite gravimetry missions on applications in hydrology, oceanography, cryosphere, solid-Earth, climate, and geodesy across various temporal and spatial scales. A comparison with uncertainties from the historical GRACE record confirms that the uncertainties of the simulated GRACE-C-like mission are of the same order of magnitude, providing confidence in the validity of the ESA-SING dataset. A global evaluation of the products shows that the NGGM and MAGIC missions will enable high-frequency (sub-weekly) observations together with significantly improved spatial resolution for 30-day and long-term products. However, NGGM-only observations, while comparable to MAGIC in performance, are limited to latitudes between $\pm 70°$ due to their inclined orbits. To address the polar gap, spherical cap regularisation is applied to NGGM-only solutions, and user recommendations are provided. Overall, the ESA-SING dataset allows users to evaluate mission-specific performance for upcoming satellite gravity missions. Its closed-loop simulations facilitate quantification of expected uncertainties in 5-day and 30-day gravity products, as well as trend and annual-cycle estimates. Moreover, the ESA SING dataset enables users to gain early experience in handling NGGM and MAGIC data and to prepare for the next generation of satellite gravimetry products.

https://doi.org/10.5194/essd-2026-672
Preprint. Discussion started: 4 November 2026
© Author(s) 2026. CC BY 4.0 License.



Open Access Earth System Science Data Discussions

1 Introduction

Satellite gravimetry missions have provided global measurements of the time-variable gravity field almost every month since 2002, enabling monitoring of mass redistribution within the Earth System at spatial scales of about 300 to 500 km. Numerous scientific disciplines have benefited from observations from the GRACE mission (Tapley et al., 2004) and its successor, GRACE-FO (Landerer et al., 2020). In particular, applications in hydrology (Rodell et al., 2018), climate science (Marti et al., 2022), cryosphere (Zemp et al., 2025), and solid-Earth (Panet et al., 2018) use the GRACE(-FO) record to document the change of our dynamic planet. In the near future, satellite missions are expected not only to extend the observational record but also to substantially improve its spatial and temporal resolution. At the end of this decade, the GRACE-C mission, developed by NASA/DLR, is planned for launch to ensure continuity of the data record from GRACE and GRACE-FO. A few years later, ESA's NGGM (Next Generation Gravity Mission) is expected to be launched (Daras, 2026, In prep.). Combining NGGM and GRACE-C observations within the Mass-change and Geoscience International Constellation (MAGIC) (Heller-Kaikov et al., 2023; Daras et al., 2023), will exploit the complementary sampling of multiple satellite pairs, an observing concept identified as a key step towards improved spatial and temporal resolution in satellite gravimetry (Pail et al., 2015).

These improvements are expected to broaden the range of processes that can be resolved with satellite gravimetry and to strengthen its contribution to both scientific applications and operational services (Kusche et al., 2025; Daras et al., 2024). Results from the ESA SING project demonstrate the potential benefits of NGGM and MAGIC across hydrology, oceanography, glaciology, climate science, solid-Earth science, and geodesy (Pfeffer et al., 2026) In particular, improved spatial and temporal sampling can enhance the characterisation of hydrological extremes and continental water storage, ocean mass redistribution and large-scale circulation, rapid mass changes in glaciers and ice sheets, and co- and post-seismic deformation. More accurate observations of mass redistribution at finer scales can additionally improve the closure of sea-level and Earth energy budgets and contribute to advances in gravity-field and geoid determination (Pfeffer et al., 2026). Realising these scientific opportunities, however, requires the community to develop and adapt analysis strategies capable of exploiting the substantially increased resolution and sampling of the forthcoming observations.

The ESA-SING dataset bridges current GRACE(-FO) observations and future mission capabilities by enabling researchers to gain practical experience with data products that reflect the resolution and error characteristics anticipated from NGGM and MAGIC. In an end-to-end simulation setup (Murböck, 2015; Schlaak and Pail, 2025), the ESA-SING dataset provides simulated products from Level-2 (L2) to Level-3 (L3) over the time period of the ESA ESM 2.0 (Dobslaw et al., 2015) incorporating realistic instrumental noise (Daras, 2026, In prep.) and background-model errors, including temporal aliasing effects (Dobslaw et al., 2016) for the three mission constellations. The goal is to enable users to prepare their processing frameworks for products of improved temporal and spatial resolution before the mission launch and to quantify how advances in the observing system translate into improved constraints on application-specific research questions.

This paper describes the ESA-SING dataset, which is publicly available at the ISDC portal (Schlaak et al., 2026). In the following, we present the simulation setup emphasising the product consistency and the assumptions underlying the ESA-SING dataset (Sect. 2). We document the applied post-processing strategies in Section 3 and provide a detailed product description

https://doi.org/10.5194/essd-2026-672
Preprint. Discussion started: 4 November 2026
© Author(s) 2026. CC BY 4.0 License.



(Sect. 4) for 5-day and 30-day products as well as direct estimates of trend and annual cycle products. To validate the dataset, the simulated uncertainties are compared to the GRACE record (Sect. 5). Furthermore, we evaluate the simulated performance differences between the missions in Section 7 and share first experiences with future mission products (Sect. 7.2).

2 Simulation environment

The simulation environment used to produce the ESA-SING dataset is based on the acceleration approach, computing the gravity field coefficients directly from gravity accelerations, a method that has been used for various mission performance assessments in the past (Murböck, 2015; Hauk et al., 2017; Schlaak and Pail, 2025). The ESA-SING dataset provides gravity products that are consistently processed within a single simulation environment, enabling an objective mission comparison. For each of the mission scenarios described in Section 2.2, gravity products of mean fields, trend and annual signal are computed in different simulation scenarios. While accounting for mission-specific instrument noise(Daras, 2026, In prep.), the simulation environment computes gravity field coefficients by forward modelling the accelerations on the observing systems caused by the gravity signal in ESM 2.0 (Dobslaw et al., 2015) and background model errors (Dobslaw et al., 2016). The resulting gravity field models are evaluated by comparing them to the target signal as a reference.

2.1 Input models

The time variable gravity field used as input model for the forward modelling consists of the target signal (Sect. 2.1.1) and the error introduced from background model errors (Sect. 2.1.2), while the retrieved signal is then compared against the reference, being the target signal averaged over the observation interval.

2.1.1 Target signal

The target signals of the simulations are the Hydrology, Ice, and Solid-Earth (HIS) components of the ESA ESM 2.0 (Dobslaw et al., 2015). The ocean (O) and atmosphere (A) components have not been restored in this dataset, as the O component includes both the manometric sea-level change and high-frequency signals that cannot be readily separated in ESM 2.0. The components of each layer of the ESM 2.0 are based on different models described in Dobslaw et al. (2015). The H component represents the Terrestrial Water Storage (TWS) anomaly simulated by the Land Surface Discharge Model (LSDM;(Dill, 2008)) forced by ERA-Interim (Dee et al., 2011), including a representation of soil moisture, snow storage, and water stored in rivers and lakes. The I component represents ice mass changes over ice sheets and mountain glaciers, expressed as surface mass anomalies in equivalent water height. Over Greenland and Antarctica, the I component includes the accumulated surface mass balance from RACMO2 (Ettema et al., 2009) forced by ERA-Interim. The ice mass dynamics are approximated using the local secular trends and low-pass-filtered signals with periods longer than 1000 days from the original ESM (Gruber et al., 2011). The ice mass changes across mountain glaciers are simulated as linear trends for Alaska, the European Alps, the Himalayas, and the Karakoram Mountain Range using the loss rates from Gruber et al. (2011) and areas from the Randolph Glacier Inventory. The S component represents Glacial Isostatic Adjustment and Co- and Post-Seismic Deformations from the original ESM,

https://doi.org/10.5194/essd-2026-672
Preprint. Discussion started: 4 November 2026
© Author(s) 2026. CC BY 4.0 License.



completed with degree-1 components (Dobslaw et al., 2014). The HIS input signal has a temporal resolution of 6 hours and covers a period of 12 years from 1995 to 2006. In the forward modelling of the simulations, the 6-hourly fields are linearly interpolated to fit the 5-second sampling of the satellite observations. To achieve appropriate reference signals for different simulation scenarios (Sect. 2.3), the target signal (HIS) is averaged over the same mean period, or in the case of the direct estimation of trend and annual signal, they are directly estimated from the 6-hourly HIS fields over the same period as the simulation scenario. In the forward modelling, the input signal is truncated at the same spherical harmonic degree and order (d/o) as the resolution of the resulting simulated gravity solution.

2.1.2 Background model errors

Temporal aliasing dominates the error in current satellite gravimetry products (Flechtner et al., 2016), it is caused by high-frequency mass transport signals that alias into the global satellite product. Therefore, tidal and non-tidal high-frequency signals are reduced with a priori knowledge in gravity field processing. For this data set, the uncertainty of the non-tidal de-aliasing model is accounted for in the simulation by introducing the AOerr error term from the ESM 2.0 (Dobslaw et al., 2016) into the forward modelling process. The tidal de-aliasing model errors are approximated by the model difference of got4.7 (Ray, 1999) and eot11a (Savcenko and Bosch, 2011). These errors in the forward model and the high-frequency components of the target signal (mainly caused by the H component), in combination with instrument noise (Sect. 2.2.2), result in the well-known meridional striping in the simulated gravity products.

2.2 Satellite constellations

The dataset contains time-variable gravity products from three satellite mission constellations, namely GRACE-C-like, NGGM, and MAGIC. While the GRACE-C-like and the NGGM constellation consist of single pair missions where a pair of low Earth orbiting satellites measures the time variable gravity field by satellite-satellite tracking measurements, MAGIC is the realisation of the combination of GRACE-C-like and NGGM observations. The mission configurations for GRACE-C-like mission and NGGM are described in the following sections with respect to the chosen orbits (Sect. 2.2.1 and Fig. 1) and instrument noise assumptions (Sect. 2.2.2).

2.2.1 Orbits

The orbits assumed in the simulations are based on the Mission Requirement Document (MRD) (Daras, 2026, In prep.) and are computed for a single repeat cycle with 5-second sampling. After 30 days, the orbits are repeated with a shifted ascending node. This leads to drift in the ground-track pattern over the 12 simulated years, while sampling remains consistent. As both orbits have a 5-daily sub-cycle, this leads to consistent sampling between 5-daily solutions as well. The osculating Keplerian elements are summarised in Table 1. The polar pair orbits with a mean altitude of 493 km and an inclination of 89°, while the inclined pair has a lower altitude of 385 km and an inclination of 69.99°.

https://doi.org/10.5194/essd-2026-672
Preprint. Discussion started: 4 November 2026
© Author(s) 2026. CC BY 4.0 License.

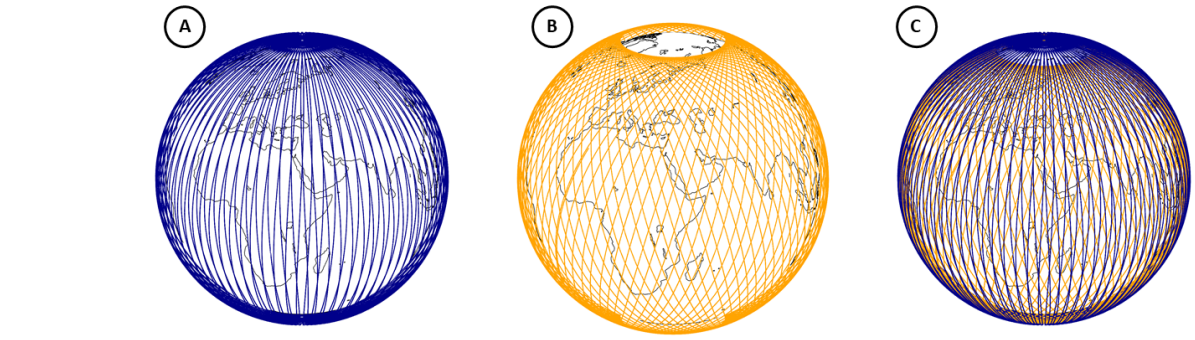


Figure 1. Ground tracks after 5 days for each Orbit configuration. GRACE-C-like ground tracks are displayed in the left column (A), NGGM in the middle column (B) and their combination, MAGIC, in the right column (C).

Table 1. Osculating Keplerian elements of the polar pair and the inclined pair for 1 Jan 2002, 00:00:00 (GPS). The leading (A) and trailing (B) satellites are shown for each pair.

	Semi-major axis [m]	**eccentricity**	**incl. [°]**	**asc. node [°]**	**argument of perigee [°]**	**mean anomaly [°]**
Polar pair-A	6871210.979	0.00160	89	359.98	27.78	331.51
Polar pair-B	6871208.124	0.00160	89	359.98	29.17	331.95
Inclined pair-A	6763724.585	0.00083	69.99	359.98	269.99	179.999999
Inclined pair-B	6763738.810	0.00083	69.99	359.98	275.32	176.531356

2.2.2 Instrument noise

Instrument noise is modelled based on the noise specifications of the accelerometers and laser ranging instruments (LRI), including tone errors. For the mission scenarios representing the GRACE-C-like and NGGM missions, the specifications of the non-gravitational acceleration uncertainties and the inter-satellite distance variation uncertainties are given in (Daras, 2026, In prep.). After propagating the uncertainties into the line of sight, an instrument noise timeseries is computed from the combined Amplitude Spectral Densities (ASD) for the accelerometer, laser-ranging instrument and tone errors (Fig. 2). This noise timeseries is added to the simulated gravity accelerations. For the GRACE-C-like mission, a superstar accelerometer and the in-orbit performance of the Laser Ranging Interferometer (LRI) at an intersatellite distance of 220 km are considered. For NGGM, the intersatellite ranging noise follows the specifications of the Laser Tracking Instrument (LTI), while the microstar accelerom-

https://doi.org/10.5194/essd-2026-672
Preprint. Discussion started: 4 November 2026
© Author(s) 2026. CC BY 4.0 License.



Open Access Earth System Science Data Discussions

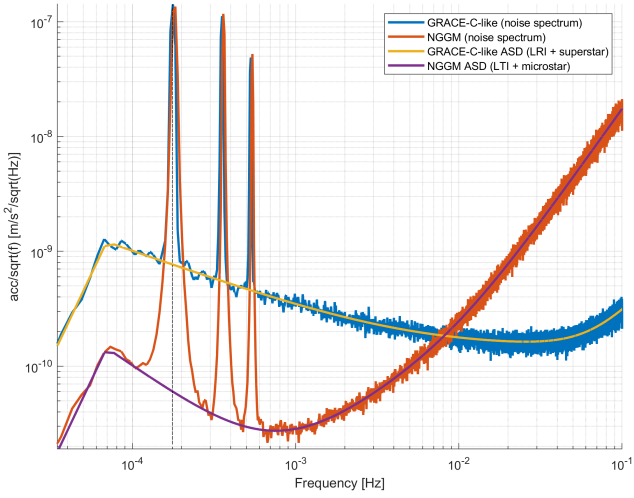


Figure 2. Combined amplitude spectral densities (ASD) of instrument uncertainties as accelerations in the line of sight.

eter specifications are used to propagate the uncertainties of non-gravitational accelerations into the simulated observations. Additionally, tone errors are considered. They are deterministic errors arising from variations in the spacecraft system, with excitation frequencies corresponding to multiples of the orbital frequencies (Müller, 2017). Following the amplitudes given in Daras (2026, In prep.), the tone errors have been entered into the simulations at three multiples of the orbital frequency, resulting in the pronounced peaks in the ASD curves in Fig. 2.

2.3 Simulation scenarios

By considering the input assumptions introduced in Sect. 2.1, long-term simulations are performed for the three constellations described in Sect. 2.2. To evaluate the relative performance of the considered missions over different temporal scales, four different parameterisation strategies are applied to recover the spherical harmonic coefficients of:

- 5-daily mean fields (max. d/o 70)
- 30-daily mean fields (max. d/o 120)
- Directly estimated trend and annual signal (max. d/o 130)
- Directly estimated trend-only signal (max. d/o 160)

Longer observation periods increase the number of observations and allow the model to achieve higher spatial resolution while keeping the adjustment system stable.

The orbits of all mission scenarios (Sect. 2.2) have a 5-day sub-cycle. Therefore, the spatial sampling is uniform, but the ground tracks appear to drift for each 5-daily solution until a full repeat cycle is reached (after 30 days). The resulting orbit

https://doi.org/10.5194/essd-2026-672
Preprint. Discussion started: 4 November 2026
© Author(s) 2026. CC BY 4.0 License.



repeat patterns imply homogeneous ground-track patterns over 5- and 30-day periods. Consequently, this dataset contains 5-daily and 30-daily mean gravity field solutions. For 5-day solutions, the temporal resolution is 5 days over 12 years. The spatial resolution corresponds to ca. 285 km (d/o 70). for monthly solutions, the temporal resolution is 30 days over 12 years, with a spatial resolution of ca. 166 km (d/o 120). For the mean-field solutions (5-daily and 30-daily), additional uncertainty information is provided as a static Variance-Covariance Matrix (VCM). The positive-definite VCM has been derived empirically in a Monte Carlo simulation setup, generating a sufficient number of samples (>20000) for an invertible VCM (Sect. 3.4).

In addition to mean fields, time-dependent components (trend and annual signal) can be estimated directly at the observation level. Over long timescales, the observation equations used to resolve trend and annual signals can be accumulated (Loomis et al., 2021; Kvas et al., 2023; Schlaak and Pail, 2025), resulting in solutions that remain stable at higher spatial resolutions. For the co-estimation of trend and annual signal, yearly normal equation systems (NEQs) are accumulated, whereas for the spatially higher-resolution trend-only estimates, 5-yearly NEQs are stacked. As background model errors increase with spatial resolution and the number of parameters creates large NEQs, the co-estimation of trend and annual signal is limited to d/o 130 (ca. 150 km), while the direct trend estimates are resolved up to d/o 160 (ca. 125 km).

3 Data products and processing steps

The database contains three data product levels derived from the end-to-end simulation outputs for the respective mission scenarios (GRACE-C-like, NGGM, and MAGIC) and simulation types (high-frequency, monthly, trend-only, and trend-and-annual) as is schematically shown in Fig. 3. Namely, the data product levels are:

- **Level 2:** filtered and unfiltered spherical harmonic coefficients in ICGEM format
- **Level 2P:** filter and unfiltered surface mass anomaly grids expressed in gridded equivalent water heights in NetCDF format, calculated from L2a and L2b data.
- **Level 3:** filter and unfiltered surface mass anomaly grids expressed in gridded equivalent water heights in NetCDF format, calculated from L2P data with post-corrections applied.

Unfiltered products are denoted by the letter "a", while VADER-filtered products (Sect. 3.2) are identified with the letter "b". The resolution of all data products (L2, L2P, L3) of each mission scenario (GRACE-C-like, NGGM, MAGIC) depends on the simulation type described in Sect. 2.3. The processing steps applied to the simulated satellite accelerations (L1) to reach the higher-level products (L2, L2P, L3) are described in the following sub-sections.

https://doi.org/10.5194/essd-2026-672
Preprint. Discussion started: 4 November 2026
© Author(s) 2026. CC BY 4.0 License.



Open Access Earth System Science Data Discussions

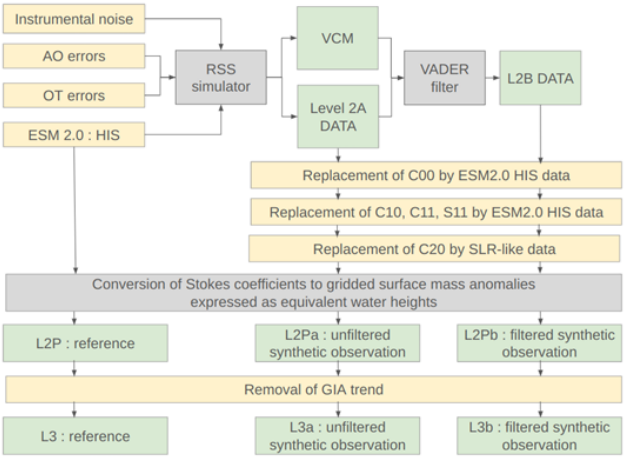


Figure 3. Schematic overview of the processing of product levels in the database. yellow boxes correspond to Input data, Grey boxes to processed data and green boxes to L2 and L3 data products

3.1 Polar gap regularisation (L1)

As described in Sect. 2.2, due to the orbit inclination, NGGM only provides a sampling of latitudes between +70° and -70°. Therefore, spherical cap regularisation needs to be introduced at the NEQ level to compensate for the polar gap and to stabilise the adjustment. While the sampling geometry improves gravity field retrieval over the covered area, it also introduces a sampling gap in polar regions. To mitigate the missing sampling over the polar regions (+/- 70° to 90°), if no other observations are available, a spherical cap regularisation has to be applied on the polar gap, similar to the processing strategies applied for the GOCE mission (Metzler and Pail, 2005).

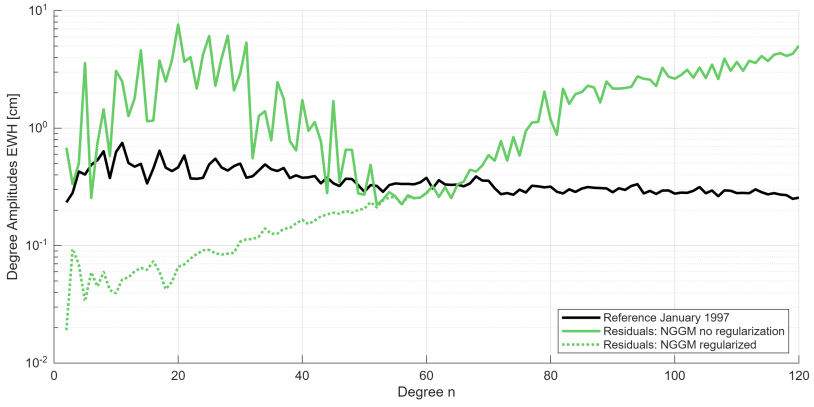


Figure 4. Degree amplitudes of an example 30-day solution (January 2000). The coefficients representing the polar areas have been removed following (Sneeuw and van Gelderen, 1997). Reference is shown in black, the residuals of the regularised NGGM solution in blue, and the residuals of the non-regularised solution in red.

https://doi.org/10.5194/essd-2026-672
Preprint. Discussion started: 4 November 2026
© Author(s) 2026. CC BY 4.0 License.



Open Access Earth System Science Data Discussions

Regularisation is implemented by introducing pseudo-observations of zero acceleration over the polar gap. These pseudo-observations are stacked to the NEQs of the NGGM observation to stabilise the solution. While this approach stabilises the adjustment significantly (Fig. 4), it introduces correlations among the zonal coefficients (see Sect. 7.2).

3.2 VADER filtering (L2b)

Level 2b products are obtained by applying a tailored VADER filter on the L2a products. The VADER filters are time variable de-correlation filters. This anisotropic filtering approach incorporates correlations obtained from a full covariance matrix (Horvath et al., 2018; Pail et al., 2022, 2023). For the products presented here, decorrelation information is taken from the formal variance-covariance matrix (VCM) obtained directly from the least-squares adjustment, which is the inverse of the normal equation system used to compute the L2a product. The filter matrix, W, is obtained from Eq. (1).

$$W = (N + \alpha M)^{-1} N \tag{1}$$

Here, N denotes the normal equation matrix. Signal information is incorporated by computing the expected signal variance of the target signal (Horvath et al., 2018). The target signal variance matrix (M) is then scaled by a scalar (α), which, in addition to the covariance information, regulates the filter strength to minimise the global residuals. This results in NGGM and MAGIC being processed with the same scaling, whereas GRACE-C-like missions require stronger filtering and, therefore, a higher filter strength to retrieve globally optimal results for 5-daily solutions. The scaling factors are summarised in Table 2.

Table 2. Scaling factors to compute VADER filters for the considered mission constellations.

	GRACE-C-like	**NGGM**	**MAGIC**
5-daily	$\alpha = 1 \times 10^{-5}$	$\alpha = 1 \times 10^{-6}$	$\alpha = 1 \times 10^{-6}$
30-daily	$\alpha = 8 \times 10^{-6}$	$\alpha = 8 \times 10^{-6}$	$\alpha = 8 \times 10^{-6}$

The L2b products are only available for 5-day and monthly products for the ESM 2.0 period of 12 years. To reduce computational effort, a representative filter was chosen for each month of the year and applied to the respective months in the time series. For 5-day solutions, a representative filter per year has been chosen. This assumption holds as the ground-track coverage is homogeneous across all periods, resulting in equally performing filtered products for the 5-daily and monthly solutions, as shown exemplarily for a MAGIC constellation in Fig. 5.

3.3 Low degrees replacement (L2)

Before the L2 (a & b) products are stored, the low degrees, C_{00}, C_{10}, C_{11}, S_{11} are replaced by the low coefficients of their respective reference due to the non-sensitivity of satellite gravimetry to these coefficients and to avoid artefacts in the simulated solutions, especially in the long-term trend residuals, that would not be present in real satellite gravimetry data. In reality, C_{00} is constant over time due to the conservation of mass (Couhert et al., 2020), which is not the case for the ESM2.0 used as input signal model in this study. C_{10}, C_{11}, and S_{11} represent the components of geocenter motion, and are usually replaced

https://doi.org/10.5194/essd-2026-672
Preprint. Discussion started: 4 November 2026
© Author(s) 2026. CC BY 4.0 License.

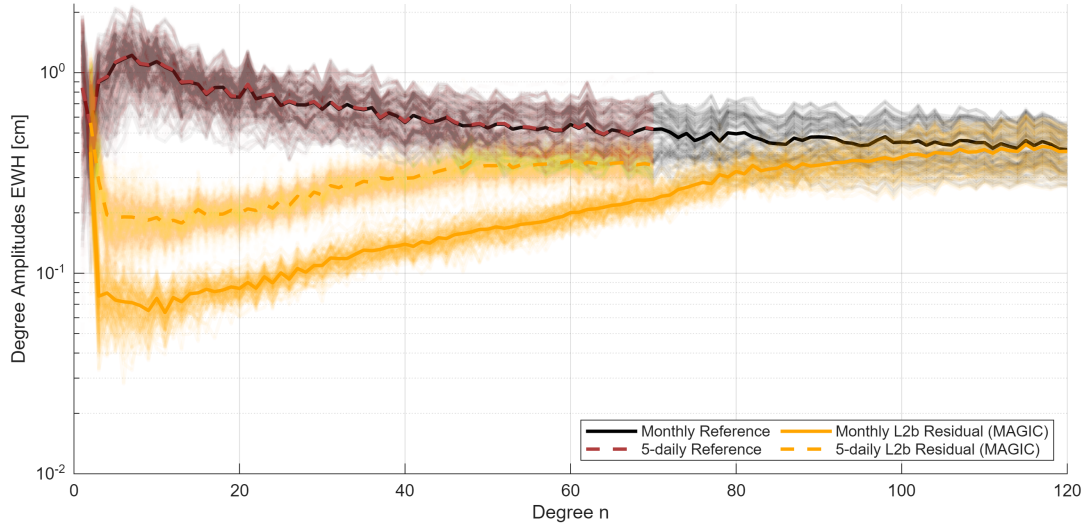


Figure 5. Degree amplitude plots in equivalent water heights in cm. The shaded lines represent the individual solutions, while the bold lines indicate the mean degree amplitudes over the ESM period 1995-2005. Solid lines represent the monthly reference signal in black and the monthly L2b residuals for the MAGIC constellation in orange up to d/o 120. The dashed lines represent the 5-daily reference signal in red and the 5-daily residuals assuming a MAGIC constellation up to d/o 70 in orange.

by model data (Swenson et al., 2008; Sun et al., 2016). However, alternatively, the low degrees can be determined by adding normal equations from satellite laser ranging observations (Lemoine et al., 2026; Daras, 2026, In prep.).

3.4 Empirical variance-covariance information

The formal errors resulting from the gravity retrieval are not representative of all error sources, as no stochastic model for the individual error sources was applied (Abrykosov and Pail, 2025; Kvas and Mayer-Gürr, 2019). However, the closed-loop simulation environment uniquely enables the computation of uncertainties for the three satellite missions by differencing the retrieved signal from the target signal. Based on these "true" errors (residuals), empirical Variance-Covariance matrices (VCMs) are computed in a Monte-Carlo setup for L2a (Eq. (2)) and L2b (Eq. (3)) products, reflecting uncertainties due to instrument noise, background model errors, and signal aliasing of 5-daily and monthly solutions.

$$\mathrm{VCM}_{\mathrm{L2a}} = \frac{1}{K-1}\sum_{k=1}^{K}\left(\hat{\mathbf{x}}(k)-\mathbf{x}_{\mathrm{ref}}(k)\right)\left(\hat{\mathbf{x}}(k)-\mathbf{x}_{\mathrm{ref}}(k)\right)^{T} \tag{2}$$

$$\mathrm{VCM}_{\mathrm{L2b}} = \frac{1}{K-1}\sum_{k=1}^{K}\left(W(k)\hat{\mathbf{x}}(k)-\mathbf{x}_{\mathrm{ref}}(k)\right)\left(W(k)\hat{\mathbf{x}}(k)-\mathbf{x}_{\mathrm{ref}}(k)\right)^{T} \tag{3}$$

K denotes the total number of samples in the Monte Carlo simulation (20000 for 5-daily and 40000 for monthly products). $\hat{\mathbf{x}}$ represents the estimated SH coefficients of sample k, while $\hat{\mathbf{x}}_{ref}$ represents the reference of sample n. In case of VCM_{L2b}

https://doi.org/10.5194/essd-2026-672
Preprint. Discussion started: 4 November 2026
© Author(s) 2026. CC BY 4.0 License.

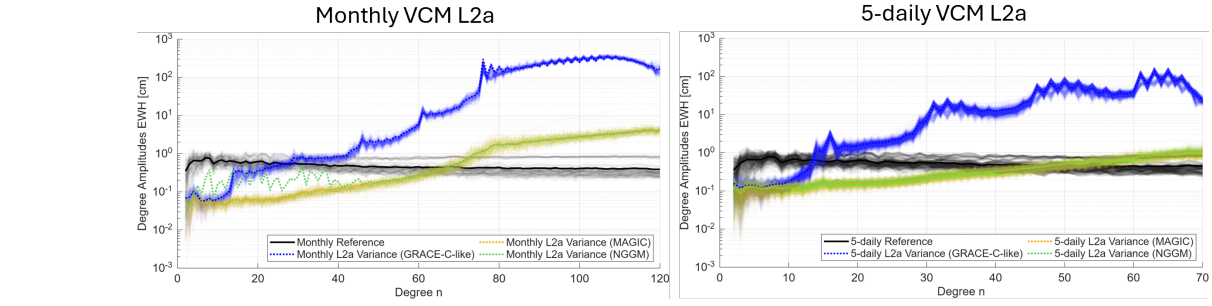


Figure 6. Degree variance plots for monthly (up to degree 120) and 5-daily (up to degree 70) L2a products that display the static variance derived from empirical VCM. As dotted lines in blue for GRACE-C-like, in green for NGGM, and in orange for MAGIC are preseted. In black, the reference signal is displayed. The residuals of the products are displayed in faded colours for the respective missions.

(see Eq. (3)), the VADER filter (W) is applied on the estimated coefficients before the residuals are computed. This approach is only possible as the ground truth is known in the simulation environment. The empirical VCMs are computed from a large number of samples (20000 - 40000), generated by shifting input signals and orbits in time. From the resulting large number of coefficient differences, which represent all error sources, a representative positive-definite empirical covariance matrix is computed.

The estimated variance of this static VCM agrees well with the mean residuals of the 5-daily and monthly solutions (Fig. 6). While the uncertainties of the VCM displayed in Fig. 6 fit well to the product residuals (displayed in faded colours of the respective mission in Fig. 6), there is one exception in the monthly variance of the NGGM L2a, which shows deviation in the low degrees compared to the residuals. This fringe effect along the polar gap in the Monte Carlo solutions is discussed in more detail in Section 6.2.

3.5 Transformation to gridded data (L2P, L3)

After filtering, the L2 data, both the unfiltered (L2a) and filtered (L2b), are transformed from spherical harmonics to gridded Equivalent Water Height (EWH) datasets. Before the transformation is applied, the C_{20} coefficients in the L2 data are replaced with C_{20} values from Satellite Laser Ranging (SLR), as is commonly done in real GRACE processing (Loomis et al., 2020). The SLR-like C_{20} time series is generated by using the C_{20} time series from the ESM 2.0 HIS signals, and adding white noise to represent the errors associated with SLR measurements. SLR C_{20} uncertainties of $\sigma_{5\text{d}} = 2 \times 10^{-11}$ and $\sigma_{30\text{d}} = \frac{2\times10^{-11}}{\sqrt{6}}$ are assumed for 5-daily and monthly solutions, respectively.

Level 2P products are generated by converting the Earth's SH coefficients (ΔC_{nm} and ΔS_{nm}) for considered degree (n) and order (m) into regularly gridded surface mass anomalies (Eq. 4), expressed as equivalent water heights using load love numbers (k_n) from Wahr et al. (1998) to the maximum degree (N_{max}).

$$\Delta\sigma(\theta,\phi) = \frac{R_e \rho_{\text{ave}}}{3} \sum_{n=0}^{N_{\text{max}}} \sum_{m=0}^{n} \bar{P}_{nm}(\cos\theta) \frac{2n+1}{1+k_n} \times (\Delta C_{nm}\cos(m\phi) + \Delta S_{nm}\sin(m\phi)) \tag{4}$$

https://doi.org/10.5194/essd-2026-672
Preprint. Discussion started: 4 November 2026
© Author(s) 2026. CC BY 4.0 License.



Considering an average density of $\rho_{\text{ave}} = 5517$ kg/m^3 and Earth's radius as $R_e = 6378.137$ m, for for points of longitude (ϕ) and colatitude(θ). Level 3 products are estimated from Level 2P products after removing the GIA trend. It is important to note that the atmosphere-ocean (AO) components of ESM2.0 have not been restored in the L2P and L3 products. As a result, the signals observed over the ocean represent only errors, including, but not limited to, ocean-tide errors, atmosphere-ocean de-aliasing errors, instrumental noise, and leakage errors. The omission error with respect to the maximum degree and order of the ESM is quantified as a grid representing the ESA ESM for the given time period from the maximum SH degree considered in the simulation type (n_{max}) until the maximum SH degree of the ESM (180). Reference Grids are truncated at the same degree and order as the respective simulation scenarios (n_{max}).

4 Data description

As described in Sect. 3, the data products are available at three levels for each of the respective mission scenarios (GRACE-C-like, NGGM, and MAGIC) and simulation type (high-frequency, monthly, trend-only, and trend-and-annual). While the L2 data is provided as SH coefficients in ICGEM files for each timestep of the simulation scenarios (Sect. 4.1), the time series for the gridded data (L2P and L3) are accumulated in netCDF files for each product level (Sect. 4.3). The accompanying uncertainty information for 5-daily and 30-daily mean products is provided as a single matrix for the products L2a and L2b (Sect. 4.2).

4.1 Spherical harmonics data

L2a and L2b products are provided as SH coefficients in ICGEM format. The header includes an extensive file description that states the input assumptions, the mission scenario and simulation type, as well as the start, end, and middle epochs of the simulated gravity field model. Following the ICGEM standard, the keywords are listed in the header (see Table 3) to define, among others, the product type, signal components, and the maximum spherical harmonic degree and order. The columns following the header include the spherical harmonic degree (N) and order (M) of the cosine (C) and sine (S) spherical harmonic coefficients of the simulation results, along with their respective residuals ($\Delta C \& \Delta S$). The residuals represent the coefficient difference between simulation results and the reference HIS signal. In case of the L2a estimates of the trend and annual signal, an additional column is added (t0 [yyyymmdd]/period [y]) in the ICGEM format to define the reference epoch of the trend or the period of the oscillating coefficients, which is one year in case of the annual estimates. The keywords in the first column follow the ICGEM standard, with 'gfc' for mean coefficients, 'gcft' for offset estimates, 'trnd' for trend coefficients and 'acos' and 'asin' for the coefficients representing amplitudes of oscillating signal components (annual).

4.2 Empirical VCM for mean products

The empirical VCMs are provided in MATLAB (.mat) format and contain two matrices. C ($C_{filtered}$, in case of L2b) corresponds to the VCM matrix, which is a square matrix with dimension length (d) dependent on the maximum degree and order of the product (n_{max}) (Eq. (5)).

$$d = (n_{\text{max}} + 1)^2 \tag{5}$$

https://doi.org/10.5194/essd-2026-672
Preprint. Discussion started: 4 November 2026
© Author(s) 2026. CC BY 4.0 License.



Open Access Earth System Science Data Discussions

Table 3. Overview of the header of ICGEM files in the database.

Keyword of the header	Example values	Description
time_period_of_data	19960225 - 19960326 (mid: 19960311)	Start date – end date (central epoch)
generating_institute	IAPG-TUM	The institute responsible for computing
begin_of_head	==========	Start of ICGEM header
Signal Components	Simulation input: HIS-AO_err+ΔOT+ϵ; Reference: HIS	Signal components of the gravity field model
product_type	gravity_field	Product type
modelname	Satellite Gravity Simulation RSS TUM 2024 - Input ESA ESM2.0	Name of the model
earth_gravity_constant	$3.98600500000 \times 10^{14}$	Gravitational constant
radius	$6.37813700000 \times 10^{6}$	Earth Radius
max_degree	120	Maximum degree and order
errors	residuals	Type of errors displayed
norm	fully_normalized	Unit of coefficients
key N M ...	Key N M C S C S t0	Table header for following data
end_of_head	==========	End of ICGEM header

To define the coefficient sequence within the VCM matrix, a variable (lmc) is also provided that lists the order of the coefficients. The first column indicates the SH degree, the second column the SH order. The third column indicates the coefficient type (0 for cos-coefficients, 1 for sin-coefficients).

4.3 Gridded data

Gridded data in this data set (L2P and L3) are provided in NetCDF format, representing a 1-degree EWH grid in millimetres. The time dimension is the third dimension of the arrays (876 for 5-daily products, 146 for monthly products), as shown in Table 4. For the simulation types trend-only and trend-and-annual, there are additional attributes for trend and annual signal amplitudes (Sim_trend, Sim_Sann, Sim_Cann) and residuals (Sim_trend, Sim_Sann, Sim_Cann) (Table 5). Each file represents a simulation type and includes all three mission constellations considered in this study over the 12 years of the ESM2.0. As an example, L2P_fivedaily_product_1995_2006.nc includes both L2Pa and L2Pb 5-daily grids of GRACE-C-like, NGGM, and MAGIC simulations from 1995 until 2006. As described in Sect. 3.5, the reference is resolved to the same maximum SH resolution as the simulation, while the effect of non-resolved SH coefficients is summarised in the omission error layer. For L3 data, additional auxiliary information is provided, containing the GIA signal removed in the simulation results and the reference.

https://doi.org/10.5194/essd-2026-672
Preprint. Discussion started: 4 November 2026
© Author(s) 2026. CC BY 4.0 License.



Open Access Earth System Science Data Discussions

Table 4. List of variables in the NetCDF files of the monthly and 5-daily products for the example of `L3_fivedaily_product_1995_2006.nc` and `L3_monthly_product_1995_2006.nc`. The same structure holds for L2P for 5-day and monthly simulation types.

Name	Long Name	Unit	Dimension (5-daily)	Dimension (monthly)
`time`	reference epoch	days (mjd)	876	146
`lat`	latitude	Degree north	180	180
`lon`	longitude	Degree east	360	360
	Reference	EWH mm	180×360×876	180×360×146
	`L3a_GRACE_C_Like_unfiltered`	EWH mm	180×360×876	180×360×146
	`L3a_NGGM_unfiltered`	EWH mm	180×360×876	180×360×146
	`L3a_MAGIC_unfiltered`	EWH mm	180×360×876	180×360×146
	`L3b_GRACE_C_Like_VADER_filtered`	EWH mm	180×360×876	180×360×146
	`L3b_NGGM_VADER_filtered`	EWH mm	180×360×876	180×360×146
	`L3b_MAGIC_VADER_filtered`	EWH mm	180×360×876	180×360×146
	Omission error	EWH mm	180×360×876	180×360×146

Table 5. List of variables in the NetCDF files of the monthly and 5-daily products for the example of `L3_fivedaily_product_1995_2006.nc` and `L3_monthly_product_1995_2006.nc`. The same structure holds for L2P for 5-day and monthly simulation types.

Name	Long Name	Unit	Dimension (5-daily)	Dimension (monthly)
`time`	reference epoch	days (mjd)	876	146
`lat`	latitude	Degree north	180	180
`lon`	longitude	Degree east	360	360
	Reference	EWH mm	180×360×876	180×360×146
	`L3a_GRACE_C_Like_unfiltered`	EWH mm	180×360×876	180×360×146
	`L3a_NGGM_unfiltered`	EWH mm	180×360×876	180×360×146
	`L3a_MAGIC_unfiltered`	EWH mm	180×360×876	180×360×146
	`L3b_GRACE_C_Like_VADER_filtered`	EWH mm	180×360×876	180×360×146
	`L3b_NGGM_VADER_filtered`	EWH mm	180×360×876	180×360×146
	`L3b_MAGIC_VADER_filtered`	EWH mm	180×360×876	180×360×146
	Omission error	EWH mm	180×360×876	180×360×146

5 Validation of simulated gravity products

The ESA SING dataset provides an extensive catalogue of satellite gravity mission simulations representing current-like and future mission scenarios, enabling application studies to assess the impact of the proposed GRACE-C-like, NGGM, and MAGIC

https://doi.org/10.5194/essd-2026-672
Preprint. Discussion started: 4 November 2026
© Author(s) 2026. CC BY 4.0 License.



missions. To evaluate the realism of these simulations, Sect. 5 compares the GRACE-C-like simulated errors against uncertainty estimates derived from the GRACE and GRACE-FO missions.

Although GRACE, GRACE-FO, and the GRACE-C-like mission all employ a single polar satellite-pair configuration and are therefore expected to exhibit similar performance, some differences remain. The GRACE and GRACE-FO satellites follow drifting orbits that do not maintain the strict repeat cycle assumed for the simulated GRACE-C-like mission. In addition, the Laser Ranging Interferometer (LRI) was flown only on GRACE-FO, whereas the original GRACE mission relied exclusively on the K-Band Ranging (KBR) instrument.

The validation focuses on barystatic sea-level change, which quantifies variations in the total amount of water mass in the ocean. Uncertainties from the GRACE and GRACE-FO missions are estimated using an adaptation of the ensemble approach proposed by Blazquez et al. (2018).

A meaningful validation requires that the simulated errors and observation-based uncertainty estimates represent the same error sources. The closed-loop simulations quantify only mission-level measurement errors, as the prescribed ground truth eliminates uncertainties introduced during subsequent post-processing. Accordingly, the ensemble analysis is restricted to Level-2 spherical harmonic solutions and excludes uncertainties associated with post-processing choices, such as degree-1 coefficients, the low-degree zonal harmonics (C_{20} and C_{30}), glacial isostatic adjustment (GIA), and spatial filtering.

The ensemble consists of five independent Level-2 solutions produced by the international processing centres CSR, JPL, GFZ, ITSG, and CNES. To ensure a consistent processing strategy, the degree-0 coefficient (C_{00}) is replaced by the negative of the atmospheric contribution from the AOD1B RL06 dealiasing model (GAA; Dobslaw et al. 2017), thereby conserving the total mass of the Earth system. The degree-1 coefficients are replaced using TN13a (Sun et al., 2016), while the C_{20} and C_{30} coefficients are substituted with Satellite Laser Ranging (SLR) estimates from TN14 (Loomis et al., 2020). Glacial isostatic adjustment is corrected using the ICE6G-D model (Peltier R. et al., 2018), and the oceanic component of the AOD1B RL06 dealiasing model (GAB) is restored (Dobslaw et al., 2017). Finally, the historical GRACE observations spanning 2005-2016 are compared with the corresponding simulation results generated for the period 1995-2006.

To ensure a consistent comparison, the simulated GRACE-C and observed GRACE and GRACE-FO gravity fields are processed using identical filtering and leakage-correction procedures. Both datasets are filtered with the standard non-isotropic DDK6 decorrelation filter (see http://icgem.gfz-potsdam.de/Visualized_DDKkernels.pdf), and the same leakage correction is applied to reassign mass variations that originate over land but are spatially smeared into the ocean back to their estimated terrestrial source regions (Lecomte et al., 2026).

After applying these common processing steps, the remaining uncertainty in the ensemble reflects only the dispersion among the five independently processed GRACE Level-2 solutions. This uncertainty is therefore expected to be more directly comparable to the mission-level errors represented in the GRACE-C-like simulations, as uncertainties introduced by post-processing have been omitted. It should be noted, however, that the ensemble approach does not capture systematic errors shared by all processing centres. Consequently, the estimated uncertainty levels likely represent a lower bound on the errors associated with the historical GRACE and GRACE-FO observations. Despite this limitation, the ensemble provides a robust first-order assess-

https://doi.org/10.5194/essd-2026-672
Preprint. Discussion started: 4 November 2026
© Author(s) 2026. CC BY 4.0 License.



ment of the realism of the simulated mission errors.

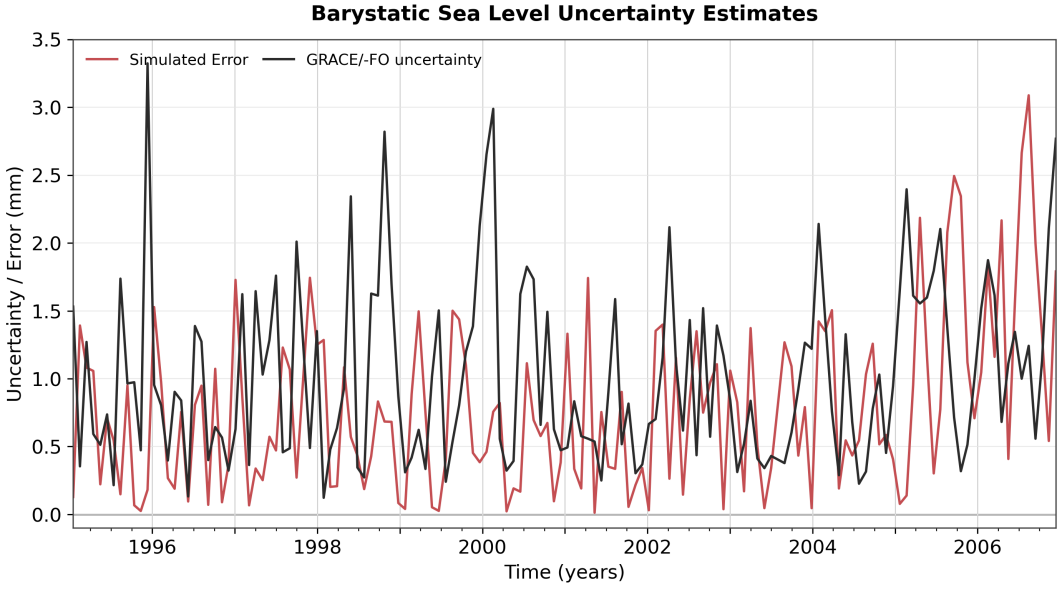


Figure 7. Barystatic sea-level simulated errors and ensemble uncertainties. The red curve displays the simulated GRACE-C-like mission error, while the black curve illustrates the historical GRACE/GRACE-FO observational uncertainty derived from the ensemble spread of five independent processing centres. Both fields are smoothed using a DDK6 filter and computed by applying a 500-km coastal buffer mask to minimise land mass leakage.

When evaluating the barystatic sea-level time series integrated over the 500-km buffered open-ocean domain, the simulated GRACE-C-like errors demonstrate a high level of consistency with the historical GRACE/GRACE-FO uncertainties derived from the ensemble approach(Fig. 7). Both time series vary with the same order of magnitude, with a temporal global mean of 1 mm for the ensemble uncertainty and 0.8 mm for the simulated error. As summarized in Table 6, the GRACE/GRACE-FO uncertainty estimates and the simulated GRACE-C-like errors show close agreement across all statistical metrics. The simulated trend error reaches 0.07 mm yr^{-1}, exhibiting an absolute difference of only 0.03 mm yr^{-1} compared to the ensemble uncertainty. Although the simulated error exhibits a lower annual amplitude (0.21 mm compared to 0.34 mm for the ensemble, representing a $\sim 38\%$ reduction), its residual variability (STD $= 0.78$ mm) remains remarkably close to the ensemble uncertainty (0.65 mm), representing a difference of only $\sim 20\%$. Overall, this strong consistency between GRACE/GRACE-FO uncertainties and GRACE-C-like errors across all metrics presented reinforces confidence in the simulation framework.

To further investigate the frequency-dependent behaviour of these signals, a Power Spectral Density (PSD) analysis was conducted (Fig. 8). The spectral curves reveal that the simulation remains highly consistent with the historical observations at high frequencies (shorter timescales encompassing sub-annual variations), showing close agreement in energy distribution.

https://doi.org/10.5194/essd-2026-672
Preprint. Discussion started: 4 November 2026
© Author(s) 2026. CC BY 4.0 License.

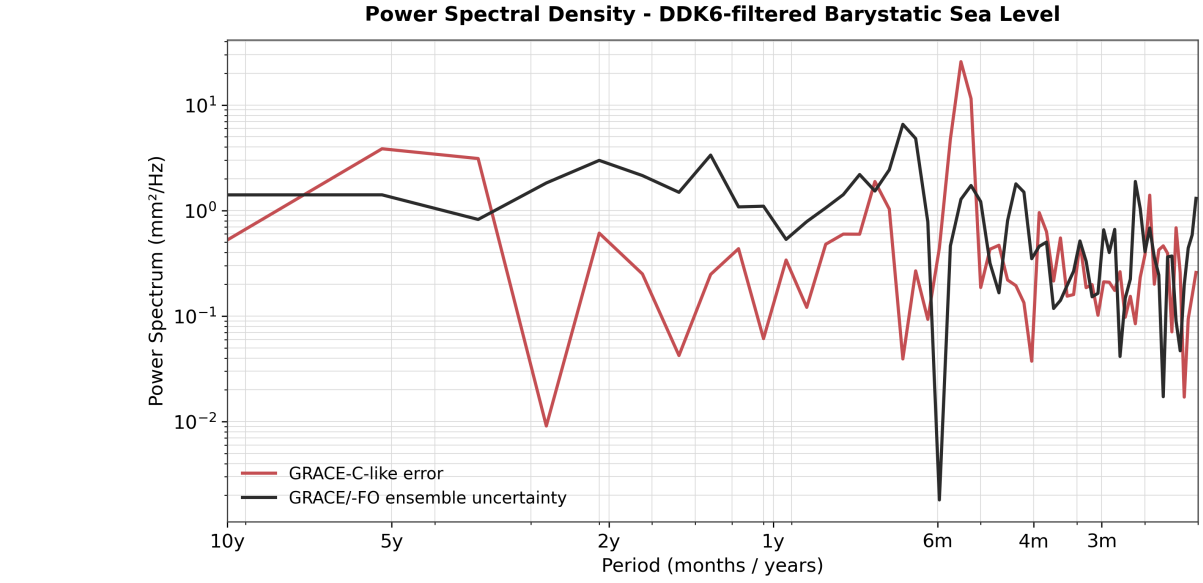


Figure 8. Power spectral density (PSD) of simulated errors and GRACE/GRACE-FO uncertainties global mean time series. PSD curves are shown for the simulated GRACE-C-like errors (black curves). These are compared against actual GRACE/GRACE-FO uncertainties in red.

Table 6. Barystatic sea-level statistical metrics comparing historical GRACE observational uncertainties and simulated GRACE-C-like errors. The metrics include the linear trend, the annual signal amplitude, and the standard deviation of the residual time series computed after removing both the trend and the annual cycle components.

Dataset	**Trend (mm yr^{-1})**	**Annual Amplitude (mm)**	**Standard Deviation (mm)**
Historical GRACE/-FO uncertainty	0.04	0.34	0.65
Simulated GRACE-C-like error	0.07	0.21	0.78

Conversely, at intermediate frequencies, corresponding to inter-annual timescales between 1 and 4 years, the simulated error spectrum reveals a noticeable energy deficit compared to the ensemble uncertainty. Several non-exclusive hypotheses can explain this lower energy level. First, the discrepancy may arise from missing dynamics in the ESM2.0 , as no ocean signals were included in the target model. As a result, correlated errors associated with interannual variability in the barystatic sea level changes are omitted in the simulations. These limitations are expected to be addressed in future developments of the Earth system model. Second, this discrepancy may stem from the idealised sampling conditions inherent to the simulation framework. While the simulations assume a strict repeat cycle and consistent temporal sampling quality—leading to overly optimistic performance on intermediate timescales (> 1 year)—the actual GRACE and GRACE-FO data records are subject to orbital drift, ground-track degradation, and observational gaps, which increase observation-based uncertainties in the GRACE/-FO ensemble. Third, potential residual errors in the simulated ocean tide models, as well as limitations in the background de-aliasing corrections (such as atmosphere and ocean de-aliasing errors), may not fully reproduce the complex, long-period aliasing pat-

https://doi.org/10.5194/essd-2026-672
Preprint. Discussion started: 4 November 2026
© Author(s) 2026. CC BY 4.0 License.


terns present in historical satellite gravity solutions. Future studies may address these limitations by incorporating improved forward models, more realistic orbital perturbations, and refined representations of tide and dealiasing errors in the simulations.

Overall, the close agreement across temporal and spectral metrics confirms that the simulation framework successfully reproduces the overall noise magnitude and variability observed in historical gravimetry missions. It provides a robust baseline for propagating future geodetic uncertainties into global ocean mass and sea-level budget assessments.

6 Mission comparison

The three mission constellations GRACE-C-like, NGGM, and MAGIC (Sect. 2.2) are planned to be launched into orbit within the next decade. GRACE-C-like simulations agree with respect to the uncertainties computed from the historical GRACE record (see sect. 5). NGGM and MAGIC introduce a better observation geometry that reduces temporal aliasing in gravity models derived from their observations. The NGGM observations have a sampling gap due to the inclined orbit (compare Sect. 2.2.1), which is treated in the processing with a polar gap regularisation (Sect. 3.1). Due to this sampling constraint, degree amplitude plots containing NGGM results will always exclude the coefficients associated with the polar gap following Sneeuw and van Gelderen (1997) (see e.g. Fig. 4). For unfiltered products (L2a and L3a), a mission comparison is straightforward, as performance is indicated by residuals across different temporal scales and the spherical harmonic spectrum (spatial scales). When filters are applied (L2b and L3b), the performance difference between the missions decreases, and the a priori knowledge entering the filter construction has a significant effect. Here, the comparison is more complex, as the filter's dampening effect must be considered alongside the apparent performance of the residuals.

6.1 Mean-field products (5-daily and monthly)

The short-term products resolve the time-variable gravity field up to d/o 70 for 5-daily averages (Sect. 2.3). The unfiltered datasets (L2a and L3a) contain the entire errors of instruments and temporal aliasing, leading to an increase in residuals for higher spherical harmonics, L2, (Fig. 9) and the well-known striping pattern in the spatial domain, L3, (Fig. 10). Comparing the missions, the reduced noise performance of NGGM and MAGIC becomes evident as the signal-to-noise ratio cross-over is reached in the monthly solutions of average at degree and order 68, while a GRACE-C-like mission already reaches the cross-over point at d/o 28. When the same simulation results are transformed onto a grid of equivalent water height (L3), these improved retrieval performances are reflected in reduced global residuals (Fig. 10).

Overall, filtered products (L2b and L3b) display significantly lower noise levels. After applying the VADER filter (Sect. 3.2), the coefficients containing noise components are reduced, but signal dampening occurs (Fig. 11), especially for localised signals of high amplitude (Fig. 12). While Fig. 11 shows that, in terms of residuals, the satellite missions appear to perform much more similarly to each other, looking at the filtered mean signal curves of the individual missions shows that the signal damping is much less in the case of NGGM and MAGIC than in the case of GRACE-C-like. Therefore, more signal content of high spatial resolution will remain in the filtered NGGM and MAGIC products in the case of monthly and 5-daily products.

https://doi.org/10.5194/essd-2026-672
Preprint. Discussion started: 4 November 2026
© Author(s) 2026. CC BY 4.0 License.

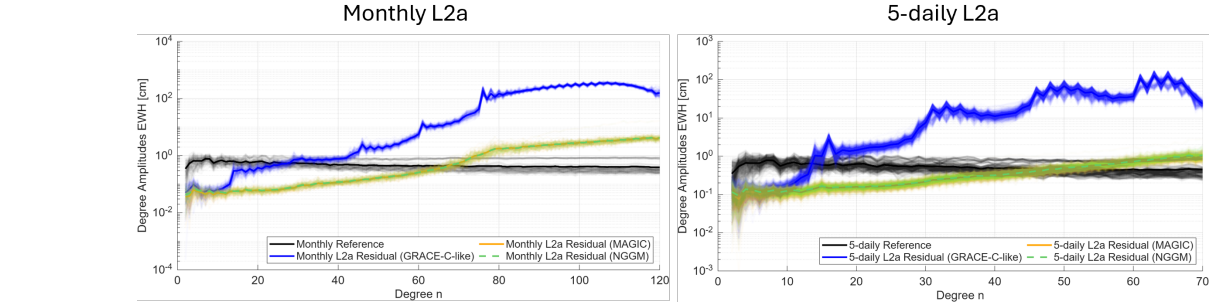


Figure 9. Mission residual comparison of unfiltered L2a for monthly (left panel) and 5-daily products (right panel). The solid lines show the average of the reference signal (black), while blue displays the mean residuals of GRACE-C-like missions, orange displays the mean residuals of a MAGIC double pair mission, and dashed green displays the NGGM mean performance. The shaded curves show the single-solution performances between 1995 and 2006. All curves are cut to the polar gap of NGGM for comparison (as if looking at $\pm 70°$ latitude in the spatial domain).

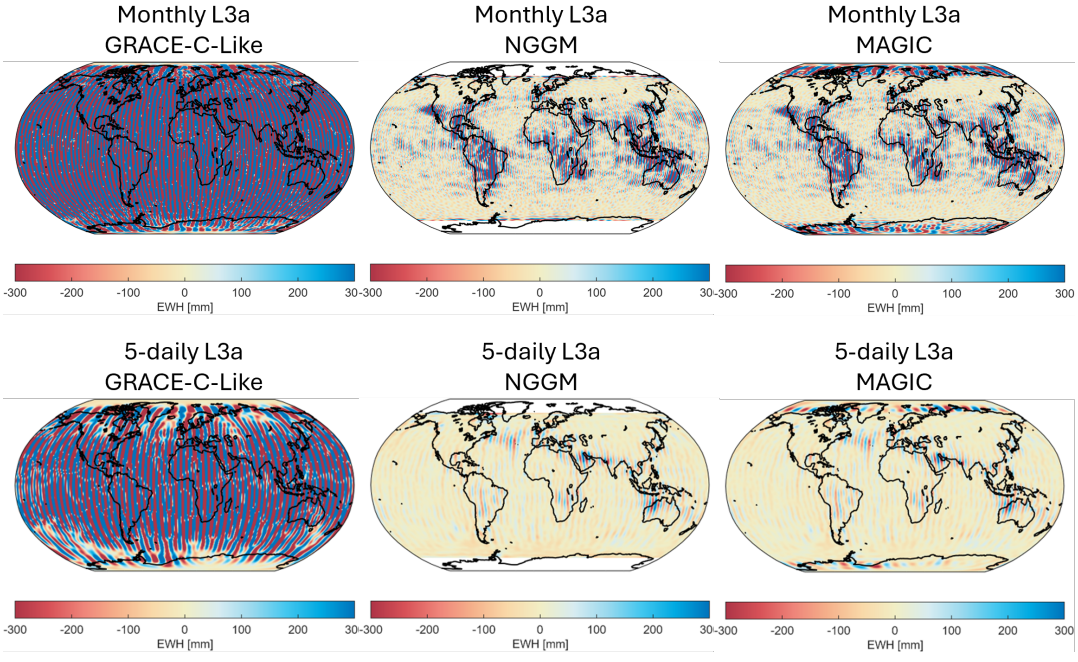


Figure 10. Mission residual comparison of unfiltered L3a products. Residuals of January 1995 are shown in the upper panel for GRACE-C-like mission (left), NGGM (middle), and MAGIC (right). The same is displayed in the lower panel for the first 5-day solution of 1995.

As mentioned in Section 3.4, the variance information, estimated from the empirical VCM, is representative for both monthly and 5-daily solutions, whether unfiltered (L2a) or filtered (L2b). However, the unfiltered variance of NGGM exhibits artefacts in the low degrees due to the spherical cap regularisation applied in the Monte Carlo simulations. The affected coefficients

https://doi.org/10.5194/essd-2026-672
Preprint. Discussion started: 4 November 2026
© Author(s) 2026. CC BY 4.0 License.

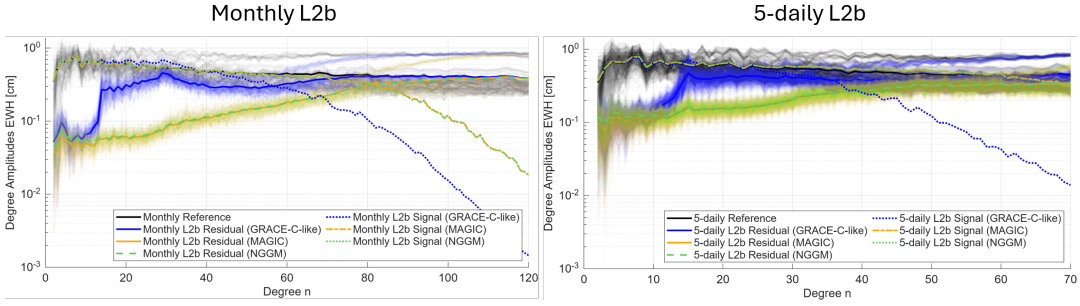


Figure 11. Mission residual comparison of filtered L2b for monthly (left panel) and 5-daily products (right panel). The solid lines show the average of the reference signal (black), while blue displays the mean residuals of GRACE-C-like missions, orange displays the mean residuals of a MAGIC double pair mission, and dashed green displays the NGGM mean performance. The shaded curves show the single-solution performances between 1995 and 2006. In addition to the L2a analysis in Fig. 9, the mean signal is plotted as dotted lines to illustrate the filtering-induced damping. All curves are cut to the polar gap of NGGM to allow comparison (similar to looking at ±70° latitude in the spatial domain).

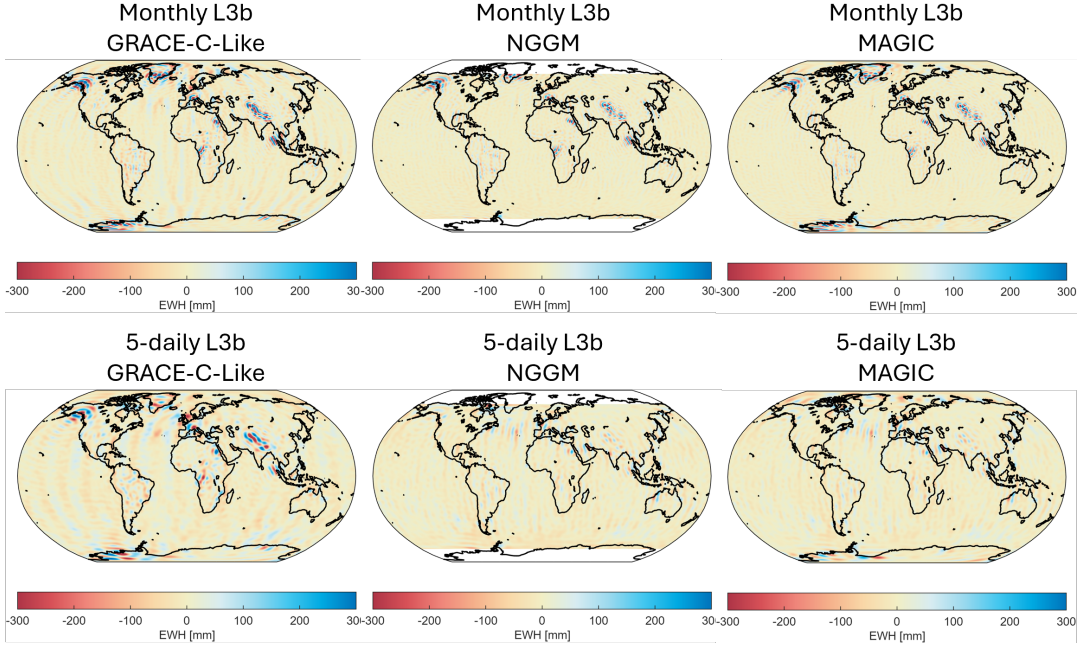


Figure 12. Mission residual comparison of filtered L3b products. Residuals of January 1995 are shown in the upper panel for GRACE-C-like mission (left), NGGM (middle), and MAGIC (right). The same is displayed in the lower panel for the first 5-day solution of 1995.

are specifically tied to the transition zone of the polar gap (Fig. 13). Since these artefacts stem from the polar regularisation, necessary to stabilise the solutions, in combination with the higher spatial resolution of the monthly solutions, they are inherent

https://doi.org/10.5194/essd-2026-672
Preprint. Discussion started: 4 November 2026
© Author(s) 2026. CC BY 4.0 License.

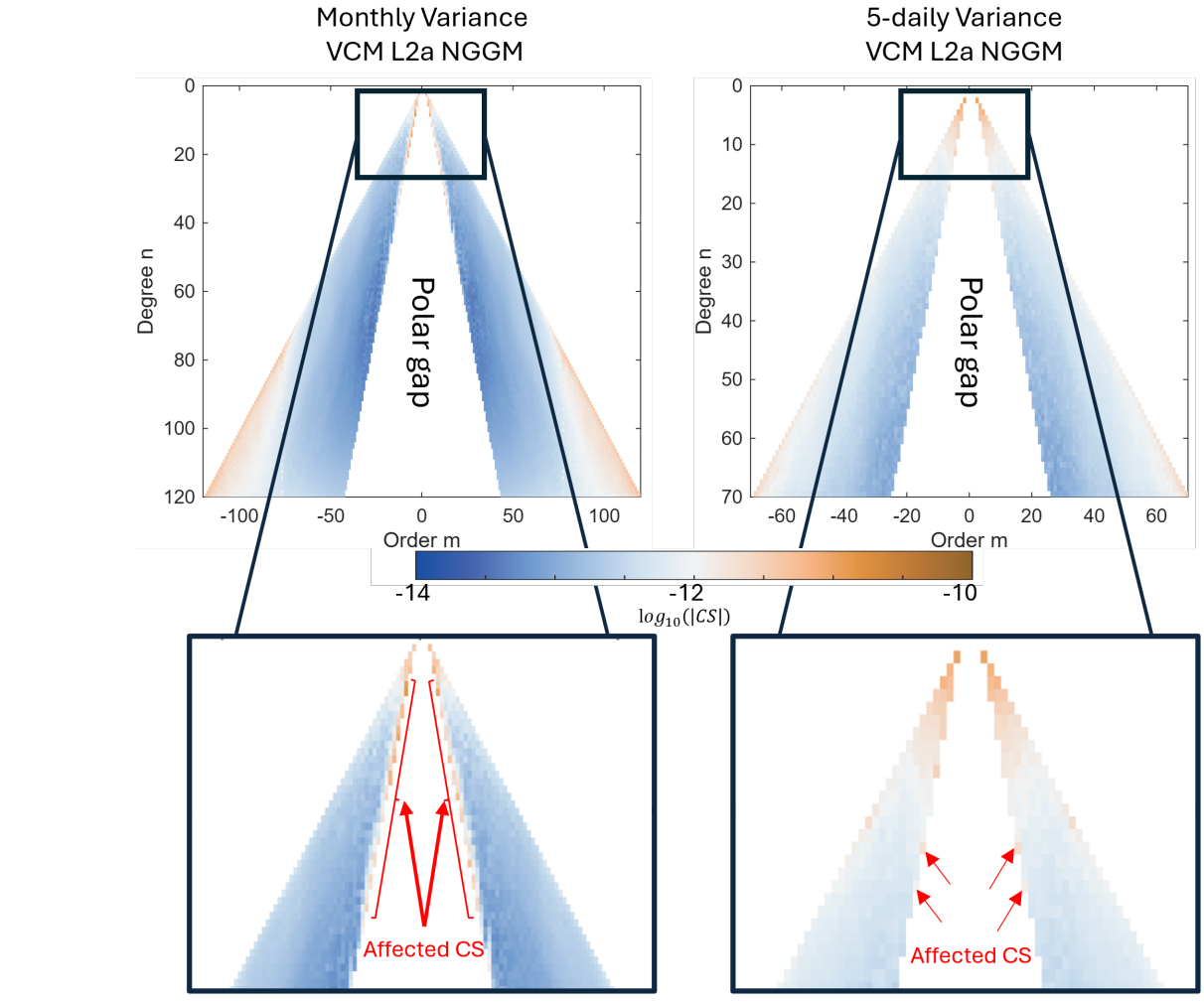


Figure 13. Triangle plots derived from the L2a VCM information of the NGGM constellation. On the left, the monthly variance is shown, and on the right, the 5-day. In the bottom row, the upper triangles are zoomed in to display the affected coefficients causing the artefacts, especially for the monthly variance.

to this method. Therefore, we recommend that users exclude a few additional polar-gap coefficients when applying the monthly unfiltered VCMs of NGGM (see Fig. 13). The effects are negligible in the case of the unfiltered 5-daily VCM (compare Fig. 6). It is important to note that the filter compensates for this issue, and the unfiltered VCMs of GRACE-C-like and MAGIC are unaffected. While this dataset computes the VCM from Monte Carlo simulations, current processing strategies aim to stochastically propagate all noise components to compute realistic product uncertainties and are not expected to exhibit these artefacts.

https://doi.org/10.5194/essd-2026-672
Preprint. Discussion started: 4 November 2026
© Author(s) 2026. CC BY 4.0 License.



6.2 Long-term trend and annual products

The long-term evaluation of the ESA-SING dataset can be investigated by looking at the direct estimates of annual amplitude and trend or computing the trend and annual amplitude from mean solutions (Sect. 2.3). In the previous section (Sect.6.2), the improved spatial and temporal resolution of NGGM and MAGIC have been shown for mean gravity models. In this section, the results are presented with respect to the long-term trend and annual amplitudes, based on monthly averages. The comparison of the impact of parameterisation strategies has already been described by Schlaak and Pail (2025). We focus here on the impact of filtering on the trend estimates from the different constellations. The long-term trend results show the improved resolution expected from NGGM and MAGIC (Fig. 14). While the noise for GRACE-C-like missions dominates the retrieved signal from d/o 60, the future missions (NGGM and MAGIC) show stable residuals almost to d/o 120 for unfiltered products. This indicates that for trend estimates, unfiltered products of MAGIC and NGGM might regionally perform better than the filtered products, as these are affected by the dampening effects of the filtering (compare right column of Fig. 14). In the case of estimates of the annual amplitude, similar observations are made. In Fig. 15, the unfiltered residuals of the three missions indicate the stable performance of NGGM and MAGIC until d/o 90, while in the case of a GRACE-C-like mission, the noise already dominates from d/o 55 onwards. As for trend estimates at certain spatial scales, the unfiltered annual amplitude will contain less noise than the errors introduced by filter damping. The spatial plots in Fig. 15 confirm that, even at higher spatial resolution, the unfiltered solution of future mission observations outperformed its filtered counterpart for annual amplitudes.

Overall, the global analysis of the residuals and mission uncertainties already highlights the potential of MAGIC and NGGM to improve the resolution of time variable gravity field models over different temporal scales from sub-weekly to decadal trend estimates. The ESA-SING dataset enables users to take these simulated uncertainties and propagate them into specific applications in a variety of topical fields, e.g., hydrology, cryosphere, ocean, climate, and solid-Earth, to highlight the impact of these missions, as well as prepare for including real observations from NGGM and MAGIC into their processing frameworks.

7 Evaluation and Recommendations

The ESA-SING dataset provides a 12-year time series of 5-day and 30-day solutions, as well as direct estimates of the long-term trend and annual amplitudes. To enable users to conduct impact studies, simulated gravity products are provided in spherical harmonics (L2) and gridded formats (L2P, L3). The unfiltered products (L2a, L2Pa, L3a) are provided alongside the VADER-filtered (compare Sect. 3.2) products (L2b, L2Pb, L3b). The residuals of the simulated products with respect to the provided reference allow direct comparison and evaluation of the mission performance of GRACE-C-like, NGGM, and MAGIC missions. The key points of global residual analysis are summarised in the following sections. Moreover, the lessons learned from the initial experience of data handling and the resulting recommendations are shared.

https://doi.org/10.5194/essd-2026-672
Preprint. Discussion started: 4 November 2026
© Author(s) 2026. CC BY 4.0 License.

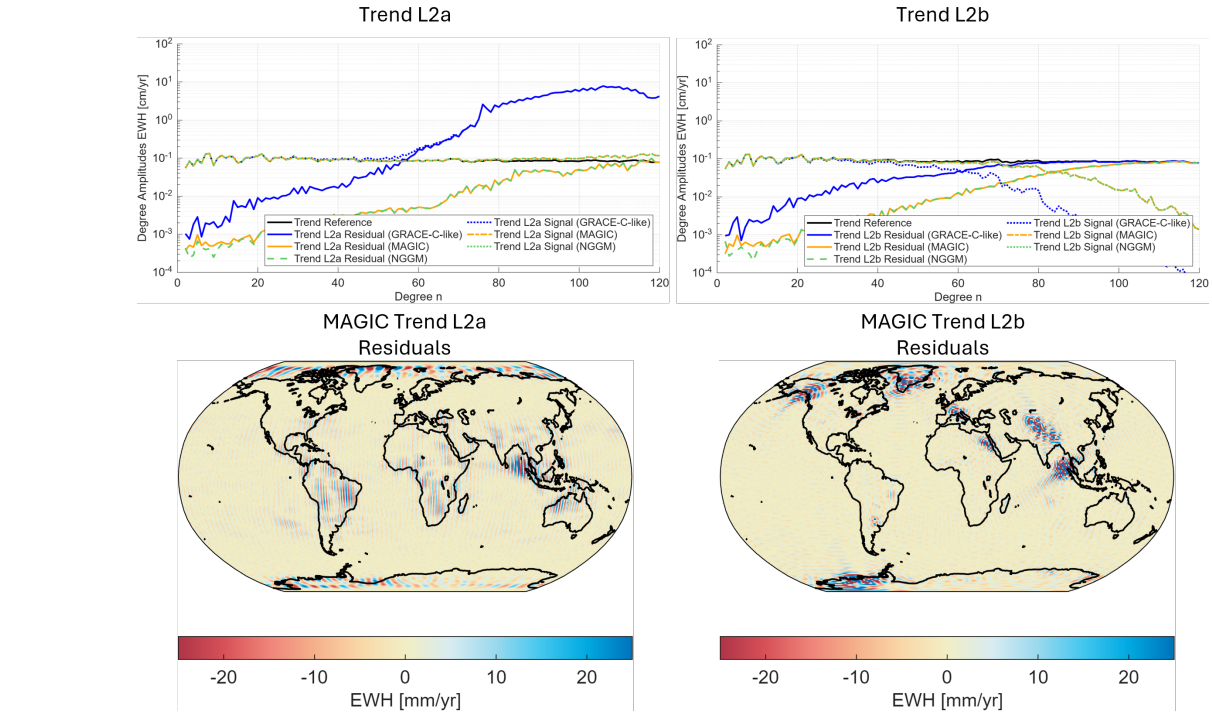


Figure 14. Long-term trend estimates based on monthly products up to degree and order 120. The top row displays mission residuals for unfiltered L2a trend estimates (top-left) and filtered L2b trend estimates (top-right). In black, the reference trend over 12 years is displayed. Solid lines indicate the residuals of GRACE-C-like (blue), NGGM (green), and MAGIC (yellow). The dashed lines indicate the retrieved signal of the respective missions. The bottom row shows the example of the trend residuals at L3 for MAGIC. The spatial pattern of the unfiltered residuals (L3a, bottom left) is shown. The effect of mainly filter damping is visible in the filtered residuals (L3b, bottom-right).

7.1 Dataset evaluation

The products presented in the ESA-SING dataset are based on the orbits described in Sect. 2.2.1, considering a consistent 5-second sampling over the period of the ESM 2.0. Instrument noise specification (Sect. 2.2.2) and background model errors (Sect. 2.1.2) are propagated from observation level for each simulation (compare Sect. 2.3) to enable users to evaluate the resulting simulated satellite gravimetry products (see Sect. 4) and their potential impact on a variety of scientific applications. The ESA-SING dataset contains consistently processed satellite products from Level 2 to Level 3 (Sect. 3), following processing strategies such as the replacement of C_{20} assuming SLR observation uncertainties. This leads to realistic uncertainties for the investigated Satellite constellations. Comparing the GRACE-C-like uncertainties from the simulations to the uncertainties expected from real GRACE data illustrates that the simulations are representative of the performance of a polar pair mission (Sect. 5).

The results show that, in a global comparison, MAGIC and NGGM are expected to significantly improve spatial resolution across all time scales and enable us to retrieve sub-weekly gravity fields at high spatial resolution. While the performance of

https://doi.org/10.5194/essd-2026-672
Preprint. Discussion started: 4 November 2026
© Author(s) 2026. CC BY 4.0 License.

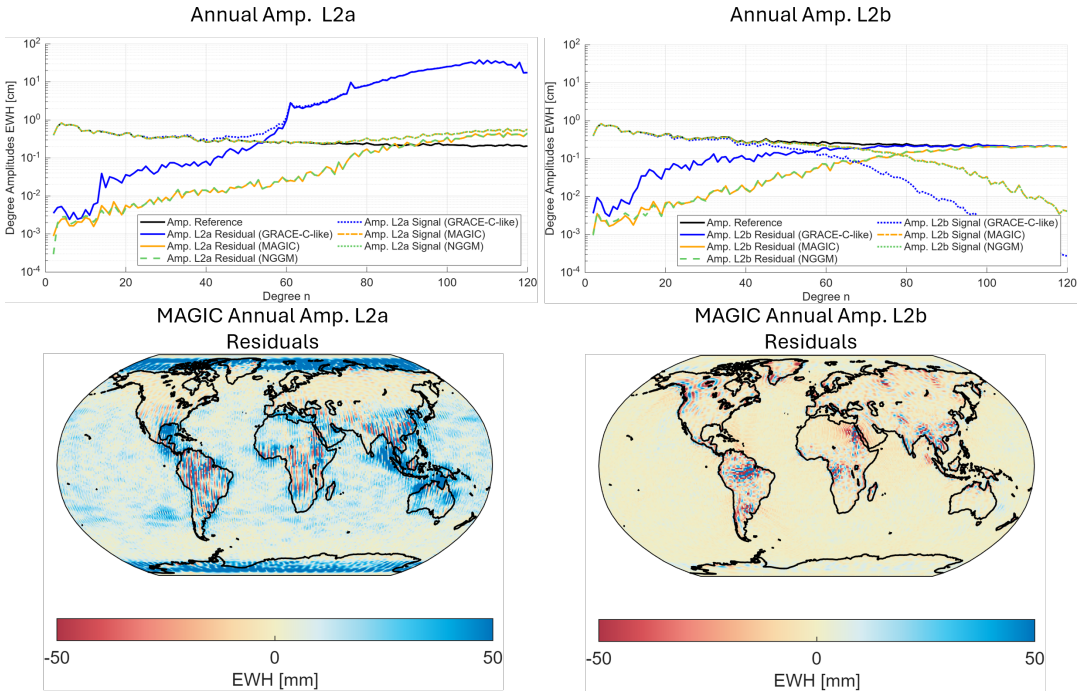


Figure 15. Annual amplitude estimates based on monthly products up to degree and order 120. The top row displays mission residuals for unfiltered L2a annual amplitude estimates (top left) and filtered L2b annual amplitude estimates (top right). In black, the reference amplitude over 12 years is displayed. Solid lines indicate the residuals of GRACE-C-like (blue), NGGM (green), and MAGIC (yellow). The dashed lines indicate the retrieved signal of the respective missions. The bottom row shows the example of the annual amplitude residuals at L3 for MAGIC. The spatial pattern of the unfiltered residuals (L3a, bottom left) is shown. The effect of mainly filter damping is visible in the filtered residuals (L3b, bottom-right).

each mission should be consistent over time due to the chosen orbit and sampling rates, there are elevated residuals visible towards the end of the ESM2.0 time series in 2005 and 2006. All mission residuals increase due to inter-annual variability within the ESM 2.0, leading to stronger signal amplitudes in the forward model (compare elevated references and residuals in Fig. 9). The elevated residuals indicate stronger signal aliasing during this period. The variance information derived from empirical VCMs obtained from Monte Carlo simulations is positive definite, making it applicable for inversion processes, e.g. in data assimilation. Comparing the provided representative VCMs agrees with the residuals computed in L2 data products, with the exception of the fringe effect appearing in NGGM monthly L2a variance (compare last paragraph of Sect. 6.2).

VADER filters are optimised for each mission scenario, taking the expected signal variance into account. Therefore, two points are worth considering. On the one hand, the filter's performance depends on the assumed signal variance. On the other hand, uncertainties in the observation system determine the required filter strength, which in turn significantly affects the signal damping introduced by the filtering process. Both have implications, too strong a weighting on the a priori will lead, in the worst case, to filtering artefacts in the products. Moreover, the stronger the filtering strength, the stronger the damping effects are

https://doi.org/10.5194/essd-2026-672
Preprint. Discussion started: 4 November 2026
© Author(s) 2026. CC BY 4.0 License.



present. This has implications for the performance assessment using residuals from filtered products. For instance, the filtered residuals might appear lower than the signal, but the filtering leads not only to reduced noise but also to a filter omission error that has to be considered, as it can significantly dampen the target signal in some applications.

7.2 Recommendations for NGGM-only data

NGGM-only simulated data are provided in the ESA-SING dataset, but due to the spherical cap regularisation over the polar gap (Sect. 3.1), some recommendations should be considered before applying the products. When displaying L2 products in terms of degree variances, the coefficients representing the polar gap should be excluded following Sneeuw and van Gelderen (1997), to avoid misinterpretation of the effect of the polar gap.

Furthermore, NGGM-only L2 products of any temporal resolution should not be truncated, as this leads to artefacts that appear as (near-) zonal ringing (Fig. 16). They result from correlations between the zonal coefficients introduced by the applied regularisation. The Vader filtered solutions (L2b products) are not as sensitive to the truncation as the high degrees are filtered, but a truncation at lower degrees can lead to similar (near-) zonal artefacts. If lower spherical degrees are required, the solutions should only be solved up to the degree to avoid these truncation artefacts.

For the computation of the empirical variance-covariance matrix (VCM) of NGGM data using the Monte Carlo approach in combination with spherical cap regularisation, fringe effects in the coefficients along the polar gap can occur (compare Fig. 13). These effects are particularly pronounced at higher spatial resolutions, such as in monthly products (d/o 120), which are more affected than 5-day solutions (d/o 70). While this effect is unavoidable, it can be attributed to the polar gap assumption when applying the variance information. Additionally, the processing strategies for real data include stochastic modelling of all noise sources, resulting in time-variable VCMs that are not expected to exhibit this effect. The Monte Carlo approach was selected here to maintain computational efficiency.

For L3 data, NGGM-only products can be handled as MAGIC and GRACE-C-like data, since the transformation to the grid has been computed to the highest resolved degree and order of the respective products in the ESA-SING dataset. But caution should be advised when interpreting the results in the transition zone around latitudes of +/- 70°, and the user should be aware that the polar regions are not observed by the mission. The values in the polar region are rather artefacts remaining from the polar gap regularisation.

8 Conclusions

The ESA-SING data consists of simulated satellite gravity products for three mission constellations: GRACE-C-like, NGGM, and MAGIC. The forward modelling of the synthetic observations is based on the ESA ESM 2.0, while instrument noise specifications and background model errors are considered. For the first time, simulated products are provided consistently over the 12-year period of the ESM for product levels L2 and L3, providing residual errors at each product level for the three mission constellations. In addition to the residual errors, uncertainty estimates for 5-day and 30-day products are provided in the form of an empirical, positive definite, variance-covariance matrix from a Montecarlo simulation set up. This data set enables

https://doi.org/10.5194/essd-2026-672
Preprint. Discussion started: 4 November 2026
© Author(s) 2026. CC BY 4.0 License.

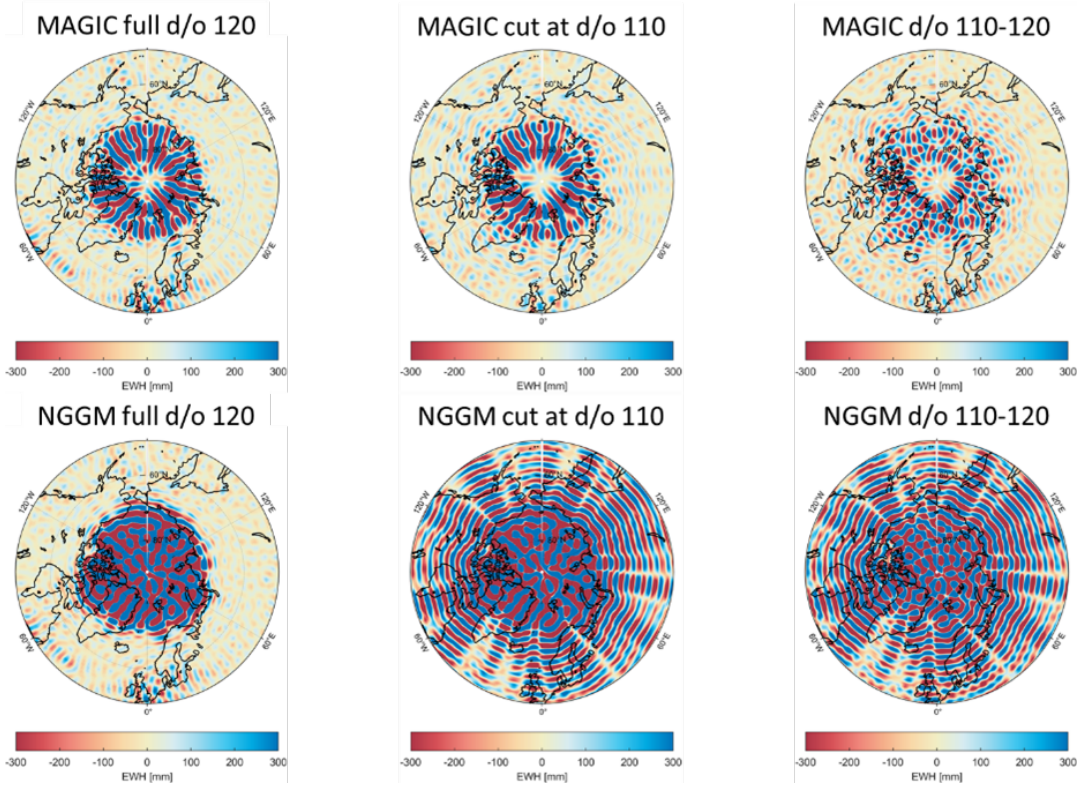


Figure 16. Comparison of L2a monthly solutions of MAGIC (upper row) and NGGM (lower row). The non-truncated solutions are displayed in the left column. The truncated solution (middle column) displays zonal artefacts that can be related to (near-) zonal coefficients of the higher degrees (right column).

users to evaluate the impact of future mission constellations on a variety of applications in hydrology, ocean, cryosphere, climate, solid-Earth, and geodesy research across temporal scales. To evaluate the derived uncertainties from this dataset, we compared them to the uncertainties from a multi-centre ensemble in the historical GRACE record. The uncertainties of the simulated polar-orbiting constellation, the GRACE-C-like mission, are of the same order of magnitude as the uncertainties in the GRACE record. This shows that the ESA-SING dataset displays realistic performance representations of the considered satellite gravimetry missions. Especially for short-term, sub-weekly products, NGGM and MAGIC will allow new observations of high-frequency processes. Furthermore, NGGM and MAGIC will enable significantly higher spatial resolution for 30-day and long-term products.

The improvements achievable with NGGM observations alone are comparable to the MAGIC performance, but are limited to latitudes between +/- 70° due to the sampling along the inclined orbit. To account for the resulting polar gap, spherical cap regularisation has to be applied in the processing of NGGM-only products, which has implications for the usage of L2 data, e.g., that the spherical harmonic series cannot simply be truncated by users on the product level.

https://doi.org/10.5194/essd-2026-672
Preprint. Discussion started: 4 November 2026
© Author(s) 2026. CC BY 4.0 License.



Overall, the ESA-SING dataset allows users to evaluate application-specific mission performances for satellite gravity missions planned in the near future. The consistent numerical closed-loop simulations enable quantification of expected uncertainties in gravity products of these missions for 5-day, 30-day, and up to 12-year products. Developing the ESA-SING dataset enables users to gain initial experience handling NGGM and MAGIC data and to prepare their frameworks for the next generation of satellite gravimetry products.

With the 2026 release of ESM3.0 (Shihora et al., 2026), the observation modelling period of the ESA ESM will be extended by an additional 14 years (2007–2020). In ESM3.0, increased dynamics are expected in the hydrology and ice layers, as well as a separate Earthquake layer. Additionally, new processes are considered, including changes in ocean bottom pressure associated with the Atlantic Meridional Overturning Circulation (AMOC), core processes, and sedimentation signals (Linus et al., 2026, In submission). To enable users to take advantage of additional considerations in the ESM 3.0 and the extended modelling period, it is planned to simulate 5-daily and monthly products, consistent with the ESA SING dataset, to provide a 26-year record of consistently simulated, GRACE-C-like NGGM and MAGIC satellite gravity products.

Data availability. The data used in this study are available through the ISDC Data Portal of the GFZ German Research Centre for Geosciences at https://isdc-data.gfz.de/. The specific dataset can be accessed directly via the following DOI: https://doi.org/10.5880/fidgeo.2026.049 (Schlaak et al., 2026)

Author contributions. Conceptualisation: MS, JP, ID, BM, Data Curation: MS, JP, Methodology: RP, ID, MS, original manuscript draft: MS, Validation: MB, AB writing, review and editing: all co-authors.

Competing interests. The authors declare that they have no conflict of interest.

Disclaimer. Copernicus Publications remains neutral with regard to jurisdictional claims made in the text, published maps, institutional affiliations, or any other geographical representation in this paper. While Copernicus Publications makes every effort to include appropriate place names, the final responsibility lies with the authors. Views expressed in the text are those of the authors and do not necessarily reflect the views of the publisher.

Acknowledgements. The work presented here was performed as part of the project ‚NGGM and MAGIC Science and Applications Impact Study‘, ESA Contract No. 4000145265/24/NL/SC, funded by the European Space Agency. We acknowledge the provision of supercomputing resources by the Leibniz Supercomputing 449 Centre (LRZ; Adress: Boltzmannstraße 1, 85748 Garching bei München, Germany).

https://doi.org/10.5194/essd-2026-672
Preprint. Discussion started: 4 November 2026
© Author(s) 2026. CC BY 4.0 License.



References

Abrykosov, P. and Pail, R.: Demonstrating the potential for the reduction of temporal aliasing through tailored stochastic modelling of non-tidal atmosphere and ocean model uncertainties in closed-loop simulations, Journal of Geodesy, 99, https://doi.org/10.1007/s00190-025-01980-4, 2025.

Blazquez, A., Meyssignac, B., Lemoine, J., Berthier, E., Ribes, A., and Cazenave, A.: Exploring the uncertainty in GRACE estimates of the mass redistributions at the Earth surface: implications for the global water and sea level budgets, Geophysical Journal International, 215, 415–430, https://doi.org/10.1093/gji/ggy293, 2018.

Couhert, A., Bizouard, C., Mercier, F., Chanard, K., Greff, M., and Exertier, P.: Self-consistent determination of the Earth's GM, geocenter motion and figure axis orientation, Bulletin Géodésique, 94, https://doi.org/10.1007/s00190-020-01450-z, 2020.

Daras, I.: Next Generation Gravity Mission (NGGM) Mission Requirements Document, 2026, In prep.

Daras, I., March, G., Mass Chnge Mission Expert Group, J., Wiese, D., Blackwood, C., Forman, F., Loomis, B., Luthcke, S., Peralta-Ferriz, C., Sauber-Rosenberg, J., Eicker, A., Panet, I., Visser, P., Meyssignac, B., Wouters, B., Bamber, J., Pail, R., and Flechtner, F.: Next Generation Gravity Mission (NGGM) Mission Requirements Document, https://doi.org/10.5270/ESA.NGGM-MRD.2023-09-v1.0, 2023.

Daras, I., March, G., Pail, R., Hughes, C. W., Braitenberg, C., Güntner, A., Eicker, A., Wouters, B., Heller-Kaikov, B., Pivetta, T., and Pastorutti, A.: Mass-change And Geosciences International Constellation (MAGIC) expected impact on science and applications, Geophysical Journal International, 236, 1288–1308, https://doi.org/10.1093/gji/ggad472, 2024.

Dee, D. P., Uppala, S. M., Simmons, A. J., Berrisford, P., Poli, P., Kobayashi, S., Andrae, U., Balmaseda, M. A., Balsamo, G., Bauer, P., Bechtold, P., Beljaars, A. C. M., van de Berg, L., Bidlot, J., Bormann, N., Delsol, C., Dragani, R., Fuentes, M., Geer, A. J., Haimberger, L., Healy, S. B., Hersbach, H., Hólm, E. V., Isaksen, L., Kållberg, P., Köhler, M., Matricardi, M., McNally, A. P., Monge-Sanz, B. M., Morcrette, J.-J., Park, B.-K., Peubey, C., de Rosnay, P., Tavolato, C., Thépaut, J.-N., and Vitart, F.: The ERA-Interim reanalysis: configuration and performance of the data assimilation system, Quarterly Journal of the Royal Meteorological Society, 137, 553–597, https://doi.org/10.1002/qj.828, 2011.

Dill, R.: Hydrological model LSDM for operational Earth rotation and gravity field variations, (Scientific Technical Report STR ; 08/09), https://doi.org/10.2312/GFZ.b103-08095, 2008.

Dobslaw, H., Bergmann, I., Dill, R., Forootan, E., Klemann, V., Kusche, J., and Sasgen, I.: Updating ESA's Earth System Model for Gravity Mission Simulation Studies : 1. Model Description and Validation, https://doi.org/10.2312/GFZ.B103-14079, 2014.

Dobslaw, H., Bergmann-Wolf, I., Dill, R., Forootan, E., Klemann, V., Kusche, J., and Sasgen, I.: The updated ESA Earth System Model for future gravity mission simulation studies, Journal of Geodesy, 89, 505–513, https://doi.org/10.1007/s00190-014-0787-8, 2015.

Dobslaw, H., Bergmann-Wolf, I., Forootan, E., Dahle, C., Mayer-Gürr, T., Kusche, J., and Flechtner, F.: Modeling of present-day atmosphere and ocean non-tidal de-aliasing errors for future gravity mission simulations, Journal of Geodesy, 90, 423–436, https://doi.org/10.1007/s00190-015-0884-3, 2016.

Dobslaw, H., Bergmann-Wolf, I., Dill, R., Poropat, L., Thomas, M., Dahle, C., Esselborn, S., König, R., and Flechtner, F.: A new high-resolution model of non-tidal atmosphere and ocean mass variability for de-aliasing of satellite gravity observations: AOD1B RL06, Geophysical Journal International, 211, 263–269, 2017.

Ettema, J., van den Broeke, M. R., van Meijgaard, E., van de Berg, W. J., Bamber, J. L., Box, J. E., and Bales, R. C.: Higher surface mass balance of the Greenland ice sheet revealed by high–resolution climate modeling, Geophysical Research Letters, 36, https://doi.org/10.1029/2009GL038110, 2009.

https://doi.org/10.5194/essd-2026-672
Preprint. Discussion started: 4 November 2026
© Author(s) 2026. CC BY 4.0 License.



Flechtner, F., Neumayer, K.-H., Dahle, C., Dobslaw, H., Fagiolini, E., Raimondo, J.-C., and Güntner, A.: What Can be Expected from the GRACE-FO Laser Ranging Interferometer for Earth Science Applications?, in: Remote Sensing and Water Resources, edited by Cazenave, A., Champollion, N., Benveniste, J., and Chen, J., vol. 55 of *Space Sciences Series of ISSI*, pp. 263–280, Springer International Publishing, Cham, ISBN 978-3-319-32448-7, https://doi.org/10.1007/978-3-319-32449-4_11, 2016.

Gruber, T., Bamber, J. L., Bierkens, M. F. P., Dobslaw, H., Murböck, M., Thomas, M., van Beek, L. P. H., van Dam, T., Vermeersen, L. L. A., and Visser, P. N. A. M.: Simulation of the time-variable gravity field by means of coupled geophysical models, Earth System Science Data, 3, 19–35, https://doi.org/10.5194/essd-3-19-2011, 2011.

Hauk, M., Schlicht, A., Pail, R., and Murböck, M.: Gravity field recovery in the framework of a Geodesy and Time Reference in Space (GETRIS), Advances in Space Research, 59, 2032–2047, https://doi.org/10.1016/j.asr.2017.01.028, 2017.

Heller-Kaikov, B., Pail, R., and Daras, I.: Mission design aspects for the mass change and geoscience international constellation (MAGIC), Geophysical Journal International, 235, 718–735, https://doi.org/10.1093/gji/ggad266, 2023.

Horvath, A., Murböck, M., Pail, R., and Horwath, M.: Decorrelation of GRACE Time Variable Gravity Field Solutions Using Full Covariance Information, Geosciences, 8, 323, https://doi.org/10.3390/geosciences8090323, 2018.

Kusche, J., Strohmenger, C., Gerdener, H., Uebbing, B., Springer, A., Ewerdwalbesloh, Y., Eicker, A., Braitenberg, C., Pastorutti, A., Pail, R., Zingerle, P., Schlaak, M., Reguzzoni, M., Rossi, L., Migliaccio, F., and Daras, I.: Benefit of MAGIC and multipair quantum satellite gravity missions in Earth science applications, Geophysical Journal International, 242, ggaf195, https://doi.org/10.1093/gji/ggaf195, 2025.

Kvas, A. and Mayer-Gürr, T.: GRACE gravity field recovery with background model uncertainties, Journal of Geodesy, 93, 2543–2552, https://doi.org/10.1007/s00190-019-01314-1, 2019.

Kvas, A., Boergens, E., Dobslaw, H., Eicker, A., Mayer-Guerr, T., and Güntner, A.: Evaluating long-term water storage trends in small catchments and aquifers from a joint inversion of 20 years of GRACE/GRACE-FO mission data, Geophysical Journal International, 236, 1002–1012, https://doi.org/10.1093/gji/ggad468, 2023.

Landerer, F. W., Flechtner, F. M., Save, H., Webb, F. H., Bandikova, T., Bertiger, W. I., Bettadpur, S. V., Byun, S. H., Dahle, C., Dobslaw, H., Fahnestock, E., Harvey, N., Kang, Z., Kruizinga, G. L. H., Loomis, B. D., McCullough, C., Murböck, M., Nagel, P., Paik, M., Pie, N., Poole, S., Strekalov, D., Tamisiea, M. E., Wang, F., Watkins, M. M., Wen, H.-Y., Wiese, D. N., and Yuan, D.-N.: Extending the Global Mass Change Data Record: GRACE Follow-On Instrument and Science Data Performance, Geophysical Research Letters, 47, e2020GL088 306, https://doi.org/https://doi.org/10.1029/2020GL088306, e2020GL088306 2020GL088306, 2020.

Lecomte, H., Blazquez, A., Fourest, S., Meyssignac, B., Pfeffer, J., Boughanemi, A., and Pellereau, É.: Leakage Corrections for GRACE Level-3 Solutions and Associated Induced Uncertainties in Manometric Sea Level Estimation, pp. 1–9, Springer Berlin Heidelberg, Berlin, Heidelberg, https://doi.org/10.1007/1345_2026_319, 2026.

Lemoine, J.-M., Bourgogne, S., Gégout, P., Reinquin, F., Marty, J.-C., Mercier, F., Loyer, S., Bruinsma, S., and Balmino, G.: 22 years of time-variable gravity field determination from GRACE and GRACE Follow-On: the CNES/GRGS RL05 solution: J.-M. Lemoine et al, Journal of Geodesy, 100, 20, 2026.

Linus, S., Volker, K., Laura, J., Robert, D., Ingo, S., Bert, W., Marius, S., Jeanne, S., Shin-Chan, H., Yoshiyuki, T., Carla, B., Muhammad Tahir, J., Gerardo, M., Hugo, L., Andrey, B., Niels, H., and Henryk, D.: Updating the ESA Earth System Model for Future Gravity Mission Simulation Studies: ESA ESM 3.0, Earth System Science Data, 2026, In submission.

Loomis, B. D., Rachlin, K. E., Wiese, D. N., Landerer, F. W., and Luthcke, S. B.: Replacing GRACE/GRACE–FO C30 With Satellite Laser Ranging: Impacts on Antarctic Ice Sheet Mass Change, Geophysical Research Letters, 47, https://doi.org/10.1029/2019GL085488, 2020.

https://doi.org/10.5194/essd-2026-672
Preprint. Discussion started: 4 November 2026
© Author(s) 2026. CC BY 4.0 License.



Loomis, B. D., Felikson, D., Sabaka, T. J., and Medley, B.: High–Spatial–Resolution Mass Rates From GRACE and GRACE–FO: Global and Ice Sheet Analyses, Journal of Geophysical Research: Solid Earth, 126, https://doi.org/10.1029/2021JB023024, 2021.

Marti, F., Blazquez, A., Meyssignac, B., Ablain, M., Barnoud, A., Fraudeau, R., Jugier, R., Chenal, J., Larnicol, G., Pfeffer, J., Restano, M., and Benveniste, J.: Monitoring the ocean heat content change and the Earth energy imbalance from space altimetry and space gravimetry, Earth System Science Data, 14, 229–249, https://doi.org/10.5194/essd-14-229-2022, 2022.

Metzler, B. and Pail, R.: GOCE Data Processing: The Spherical Cap Regularization Approach., ud Geophys Geod, 49, 441–462, https://doi.org/10.1007/s11200-005-0021-5, 2005.

Müller, V.: Design considerations for future geodesy missions and for space laser interferometry, https://doi.org/10.15488/9029, 2017.

Murböck, M.: Virtual Constellations of Next Generation Gravity Missions, Dissertation, Technische Universität München, München, 2015.

Pail, R., Bingham, R., Braitenberg, C., Dobslaw, H., Eicker, A., Güntner, A., Horwath, M., Ivins, E. R., Longuevergne, L., Panet, I., and Wouters, B.: Science and User Needs for Observing Global Mass Transport to Understand Global Change and to Benefit Society, Surveys in Geophysics, 36, 743–772, https://doi.org/10.1007/s10712-015-9348-9, 2015.

Pail et al.: NGGM/MAGIC – Science Support Study during Phase A, Final Report, ESA/ESTEC Contract Nr. 4000134613/21/NL/FF/ab., 2022.

Pail et al.: CCN1 NGGM/MAGIC - Science Support Study During Phase A "ATBD of NGGM/MAGIC L2 and L3 products", Issue 2.0, Oct 2023, ESA/ESTEC Contract Nr. 4000134613/21/NL/FF/ab., 2023.

Panet, I., Bonvalot, S., Narteau, C., Remy, D., and Lemoine, J.-M.: Migrating pattern of deformation prior to the Tohoku-Oki earthquake revealed by GRACE data, Nature Geoscience, 11, 367–373, https://doi.org/10.1038/s41561-018-0099-3, 2018.

Peltier R., W., Argus, D. F., and Drummond, R.: Comment on "An Assessment of the ICE-6G_C (VM5a) Glacial Isostatic Adjustment Model" by Purcell et al., Journal of Geophysical Research: Solid Earth, 123, 2019–2028, https://doi.org/https://doi.org/10.1002/2016JB013844, 2018.

Pfeffer, J., Meyssignac, B., Bingham, R., Blazquez, A., Bouih, M., Braitenberg, C., Brocca, L., Dobslaw, H., Ferrari, R., Forootan, E., Gerdener, H., Javed, M. T., Jensen, L., Klemann, V., Kremer, A., Kusche, J., Larnicol, G., Liaqat, M. U., Leopardi, F., Mamagiannou, E.-M., Maurizio, G., Pail, R., Panet, I., Papanikolaou, T., Saemian, P., Sasgen, I., Schumacher, M., Schlaak, M., Shihora, L., Sobouti, A., Sneeuw, N., Tourian, M. J., Tsoulis, D., Vergos, G., Wouters, B., Yang, F., and Daras, I.: Impact of the NGGM and MAGIC future satellite gravity missions for scientific applications and operational services, EGUsphere, 2026, 1–53, https://doi.org/10.5194/egusphere-2026-4642, 2026.

Ray, R. D.: A global ocean tide model from TOPEX/POSEIDON altimetry: GOT99. 2, National Aeronautics and Space Administration, Goddard Space Flight Center, 1999.

Rodell, M., Famiglietti, J. S., Wiese, D. N., Reager, J. T., Beaudoing, H. K., Landerer, F. W., and Lo, M.-H.: Emerging trends in global freshwater availability, Nature, 557, 651–659, https://doi.org/10.1038/s41586-018-0123-1, 2018.

Savcenko, R. and Bosch, W.: EOT11a-a new tide model from Multi-Mission Altimetry, in: Proceedings of the OSTST Meeting, pp. 19–21, 2011.

Schlaak, M. and Pail, R.: Resolving climate-related mass transport trends: a parameter model comparison using closed-loop simulations of current and future satellite gravity missions, Earth, Planets and Space, 77, https://doi.org/10.1186/s40623-025-02239-0, 2025.

Schlaak, M., Pfeffer, J., and Pail, R.: Simulated L2 and L3 products for impact studies of the NGGM and MAGIC gravity missions, https://doi.org/10.5880/fidgeo.2026.049, 2026.

https://doi.org/10.5194/essd-2026-672
Preprint. Discussion started: 4 November 2026
© Author(s) 2026. CC BY 4.0 License.



Shihora, L., Klemann, V., Jensen, L., Dill, R., Sasgen, I., Wouters, B., Sauber, J., Han, S.-C., Tanaka, Y., Braitenberg, C., Javed, M. T., Maurizio, G., Lecomte, H., Babeyko, A., Hovius, N., and Dobslaw, H.: The ESA Earth System Model 3.0, https://doi.org/10.5880/GFZ.UEOS.2026.001, 2026.

Sneeuw, N. and van Gelderen, M.: The polar gap, vol. 1997, p. 559–568, Springer-Verlag, 1997.

Sun, Y., Riva, R., and Ditmar, P.: Optimizing estimates of annual variations and trends in geocenter motion and J2 from a combination of GRACE data and geophysical models, Journal of Geophysical Research: Solid Earth, 121, 8352–8370, https://doi.org/10.1002/2016JB013073, 2016.

Swenson, S., Chambers, D., and Wahr, J.: Estimating geocenter variations from a combination of GRACE and ocean model output, Journal of Geophysical Research: Solid Earth, 113, https://doi.org/10.1029/2007JB005338, 2008.

Tapley, B. D., Bettadpur, S., Ries, J. C., Thompson, P. F., and Watkins, M. M.: GRACE Measurements of Mass Variability in the Earth System, Science, 305, 503–505, https://doi.org/10.1126/science.1099192, 2004.

Zemp, M., Jakob, L., Dussaillant, I., Nussbaumer, S. U., Gourmelen, N., Dubber, S., Geruo A, Sahra Abdullahi, Liss Marie Andreassen, Etienne Berthier, Atanu Bhattacharya, Alejandro Blazquez, Laura F. Boehm Vock, Tobias Bolch, Jason Box, Matthias H. Braun, Fanny Brun, Eric Cicero, William Colgan, Nicolas Eckert, Daniel Farinotti, Caitlyn Florentine, Dana Floricioiu, Alex Gardner, Christopher Harig, Javed Hassan, Romain Hugonnet, Matthias Huss, Tómas Jóhannesson, Chia-Chun Angela Liang, Chang-Qing Ke, Shfaqat Abbas Khan, Owen King, Marin Kneib, Lukas Krieger, Fabien Maussion, Enrico Mattea, Robert McNabb, Brian Menounos, Evan Miles, Geir Moholdt, Johan Nilsson, Finnur Pálsson, Julia Pfeffer, Livia Piermattei, Stephen Plummer, Andreas Richter, Ingo Sasgen, Lilian Schuster, Thorsten Seehaus, Xiaoyi Shen, Christian Sommer, Tyler Sutterley, Désirée Treichler, Isabella Velicogna, Bert Wouters, Harry Zekollari, and Whyjay Zheng: Community estimate of global glacier mass changes from 2000 to 2023, Nature, 639, 382–388, https://doi.org/10.1038/s41586-024-08545-z, 2025.